Published in final edited form as:
Cancer Res. 2021 July 01; 81(13): 3480–3494. doi:10.1158/0008-5472.CAN-20-2936.

Loss of SDHB promotes dysregulated iron homeostasis, oxidative stress and sensitivity to ascorbate

Judith Goncalves[1,2], **Sophie Moog**[#1,2], **Aurélie Morin**[#1,2], **Géraldine Gentric**[3], **Sebastian Müller**[4], **Alexander P. Morrell**[5], **Katarina Kluckova**[6], **Theodora J. Stewart**[7], **Cynthia L. Andoniadou**[8], **Charlotte Lussey-Lepoutre**[1,9], **Paule Bénit**[10], **Alpesh Thakker**[6], **Lisa Vettore**[6], **Jennie Roberts**[6], **Raphaël Rodriguez**[4], **Fatima Mechta-Grigoriou**[3], **Anne-Paule Gimenez-Roqueplo**[1,2,11], **Eric Letouzé**[12], **Daniel A. Tennant**[6], **Judith Favier**[1,2,$]

[1]PARCC, INSERM UMR970, Equipe Labellisée par la Ligue contre le Cancer, F-75015 Paris, France

[2]Université de Paris, Paris, France

[3]Institut Curie, Stress and Cancer Laboratory, Equipe Labellisée par la Ligue Nationale contre le Cancer, Inserm U830, PSL Research University; Inserm, U830, 26, rue d'Ulm, F-75005 Paris France

[4]Chemical Biology of Cancer Team, Equipe Labellisée par la Ligue Contre le Cancer. PSL Research University, CNRS UMR3666 -INSERM U1143, Institut Curie, F-75005 Paris, France

[5]Centre for Oral, Clinical & Translational Sciences, Faculty of Dentistry, Oral and Craniofacial Sciences, King's College London, UK

[6]Institute of Metabolism and Systems Research, University of Birmingham, Edgbaston, Birmingham, B15 2TT. UK

[7]London Metallomics Facility, King's College London and Imperial College London, London, UK

[8]Centre for Oral, Clinical & Translational Sciences, Faculty of Dentistry, Oral and Craniofacial Sciences, King's College London

[9]Sorbonne Université, Pitie-Salpêtrière Hospital, Department of Nuclear Medicine, Assistance Publique-Hôpitaux de Paris,F-75013, Paris, France

[10]Université de Paris, INSERM, UMR 1141, Hôpital Robert Debré, Paris, France

[$]**Correspondence to:** Dr Judith Favier Genetics and Metabolism of Rare Cancers team INSERM, UMR970 Paris-Cardiovascular Research Center 56 rue Leblanc, 75015 Paris, France Phone: +33 1 53 98 80 45 judith.favier@inserm.fr.

Author contributions

J.F., E.L. and D.A.T conceived the study. J.G., A.M., G.G., S.M., C.L.A. designed and performed the experiments, and analyzed the data. S.Mo., K.K., A.P.M., T.J.S., C.L-L., P.B. and A.T. performed the experiments and analyzed the data. J.F., D.A.T., E.L., F.M-G. and R.R. designed the experiments and analyzed the data. J.F. and A-P.G-R. supervised the study. J.F. and J.G. contributed to the management of the project, wrote the manuscript and prepared the figures. E.L. and D.A.T. contributed to the preparation of the manuscript. All the authors discussed the results and reviewed the manuscript.

Conflict of interest disclosure statement: the authors declare no potential conflicts of interest

Statement of significance

Loss of different succinate dehydrogenase subunits can lead to different cell and tumor phenotypes, linking stronger 2-OG-dependent-dioxygenases inhibition, iron overload, and ROS accumulation following SDHB mutation.

Europe PMC Funders Author Manuscripts

[11]Assistance Publique-Hôpitaux de Paris, Hôpital Européen Georges Pompidou, Department of Genetics, F-75015 Paris, France

[12]Centre de Recherche des Cordeliers, Sorbonne Université, Université de Paris, INSERM, Equipe Labellisée par la Ligue Nationale contre le Cancer, F-75006, Paris France

[#] These authors contributed equally to this work.

Abstract

Succinate dehydrogenase is a key enzyme in the tricarboxylic acid cycle and the electron transport chain. All four subunits of succinate dehydrogenase are tumor suppressor genes predisposing to paraganglioma, but only mutations in the SDHB subunit are associated with increased risk of metastasis. Here we generated an *Sdhd* knockout chromaffin cell line and compared it to *Sdhb*-deficient cells. Both cell types exhibited similar SDH loss of function, metabolic adaptation, and succinate accumulation. In contrast, *Sdhb-/-* cells showed hallmarks of mesenchymal transition associated with increased DNA hypermethylation and a stronger pseudo-hypoxic phenotype compared to *Sdhd-/-* cells. Loss of SDHB specifically led to increased oxidative stress associated with dysregulated iron and copper homeostasis in the absence of NRF2 activation. High-dose ascorbate exacerbated the increase in mitochondrial reactive oxygen species, leading to cell death in *Sdhb-/-* cells. These data establish a mechanism linking oxidative stress to iron homeostasis that specifically occurs in SDHB deficient cells and may promote metastasis. They also highlight high-dose ascorbate as a promising therapeutic strategy for SDHB-related cancers.

Keywords

metastatic paraganglioma; *SDHB* ; iron homeostasis; oxidative stress; ascorbate

Introduction

Succinate dehydrogenase (SDH) is a key enzyme localized in the inner mitochondrial membrane where it participates both in the tricarboxylic acid (TCA) cycle and the electron transport chain (ETC), as complex II. In the TCA cycle, SDH catalyzes the oxidation of succinate into fumarate while in the ETC, it allows the transfer of electrons from succinate to the ubiquinone pool. SDH is constituted of two anchoring subunits (SDHC, SDHD) and two catalytic subunits (SDHA, SDHB) encoded by the four *SDHx* nuclear genes (*SDHA*, *SDHB*, *SDHC* and *SDHD*). SDHA is a flavoprotein to which the substrate succinate binds in order to be oxidized to fumarate, while the resulting electrons are channeled to ubiquinone, through the three Fe-S clusters of SDHB. Since the initial discovery of *SDHD* mutations in 2000(1), all four *SDHx* genes have been demonstrated to act as tumor-suppressor genes (2,3,4). Their mutations predispose to pheochromocytoma and paraganglioma (PPGL), rare neuroendocrine tumors arising from chromaffin cells of the adrenal medulla and from the sympathetic and parasympathetic nervous systems, respectively; as well as gastro-intestinal stromal tumors (GIST) and rare forms of renal cell carcinomas. It is now estimated that mutations in *SDHx* genes stand for almost 50% of inherited cases of PPGL. Interestingly, *SDHB* mutations have been shown to be the highest risk factor of malignancy in patients with PPGL: approximately 50% of PPGL patients carrying *SDHB* mutations will ultimately

develop a metastatic form of the disease and a germline mutation in *SDHB* is found in up to 36% of all metastatic PPGL cases (5). In contrast, metastatic forms of the disease are found in only 5% of patients with an *SDHD* gene mutation. Moreover, *SDHB* mutated cancers are more aggressive than non-mutated metastatic ones. The overall survival of patients with metastatic *SDHB*-related PPGL was initially estimated at 42 months after diagnosis of the first metastasis versus 244 months for patients with a metastatic PPGL but without an *SDHB* gene mutation (6). Interestingly, recent studies have revealed that increased follow-up of patients with genetically determined PPGL has significantly improved their survival, demonstrating the beneficial impact of genetic testing in these patients (7,8).

In all cases, germline *SDHx* mutations are associated with loss of heterozygosity, which causes the complete loss of SDH function in the tumor (9) and a subsequent accumulation of its substrate, succinate (10). Succinate (as other TCA cycle intermediates such as fumarate and 2-hydroxyglutarate) is considered as an oncometabolite, driving aberrant activation of transcription factors and global epigenetic reprogramming. Indeed, high steady-state levels of these metabolites are known to inhibit 2-oxoglutarate (2-OG) dependent dioxygenases, such as the hypoxia-inducible transcription factor (HIF) prolyl-hydroxylases (PHDs) and Ten-eleven translocation (TET) DNA demethylases (11). These enzymes belong to the large family of iron (Fe) and 2-OG-dependent dioxygenases, which activity is based on the use of iron (12), oxygen (13) and ascorbate (14) as main co-factors. Inhibition of PHDs promotes the abnormal stabilization, and thus activity of HIF1 and HIF2, while TET inhibition leads to a lack of DNA demethylation, resulting in pseudo-hypoxic and hypermethylator phenotypes, respectively. These observations were initially revealed in genomic studies performed on large PPGL tumor collections, resulting in a better understanding of the mechanisms of SDH-related tumorigenesis. In these studies, all *SDHx* and *FH* mutated tumors clustered together, showing a transcriptome signature characterized by activation of the hypoxic response pathway (2, 15, 16) and a DNA hypermethylator phenotype (17). Despite this apparent homogeneity, some differences have emerged suggesting that *SDHB*-mutated tumors may display a particularly marked hypermethylator phenotype associated with hallmarks of neuroendocrine-to-mesenchymal transition (NMT), which were not observed in other types of *SDHx*-mutated cases (i.e *SDHA*, *SDHC* and *SDHD* mutated) (18). In order to decipher these mechanisms at the cellular level, we have generated an immortalized mouse chromaffin cell (imCC) line knocked-out for the *Sdhb* gene (17). In these cells, we showed that *Sdhb*-deficiency does promote a marked hypermethylator phenotype mediated by TET1 and/or TET2 blockade, which acts in synergy with HIF2 activation to promote NMT and metastatic dissemination (19, 20). *Sdhb-/-* cells also undergo significant metabolic reprogramming becoming critically dependent on aspartate synthesis as a major source of carbon for anabolic purposes, which supports their viability and proliferation, maintained mainly through reductive carboxylation (21).

Despite these important advances in the understanding of the oncogenic consequences of SDHB loss of function, the exact cause of the metastatic phenotype of *SDHB*-related tumors remain mostly unexplained. *SDHA* and *SDHC* mutations are rare in PPGL patients, probably because of low penetrance of the disease in mutation carriers. In contrast, *SDHB* and *SDHD* are the most frequently described mutations in PPGL, with an incidence of 8-10 and 5-7% among all PPGL cases, respectively (22). Genotype-phenotype correlation studies

performed in patients with *SDHB* or *SDHD* mutations have undoubtedly demonstrated their different clinical behavior in terms of invasiveness. To address this crucial question in the field, we have generated *Sdhd* knocked-out cell lines in the imCC model. In this new and unique model, we have investigated the different pathways previously identified in SDH-related tumors in order to identify the specificities that may explain their different clinical behavior.

Materials and Methods

Detailed methods are provided in the Supplementary Information section.

Sdhd KO, Sdhd-rescue cell generation and cellular analysis

Complete knock-out of *Sdhd* gene was achieved in immortalized mouse Chromaffin Cells (imCC) by transfecting Wild-Type imCC, previously generated by our lab (17), with *in silico* designed targeted gRNA, using the PrecisionX Cas9 SmartNuclease RNA system kit (System Biosciences). *Sdhd*-rescue clones were established by transfecting *Sdhd*-/- imCC with an SDHD-expressing vector (ORIGENE, NM003002). Screening of these clones was performed by SDH activity test, qRT-PCR and direct sequencing of the *Sdhd* gene by Sanger method. Cells used for experiments were maintained in DMEM high glucose Glutamax (Gibco) unless when grown for metabolic or respirometry experiments (see Supplementary Information). Wound scratch assays, proliferation and adhesion tests were performed to assess cellular phenotype. When stated, cells were treated with indicated doses of iron Chloride (Sigma), MitoTEMPO (Sigma), L-Ascorbic acid (Sigma), Talazoparib (MedChemTronica) or N-acetyl-cysteine (Sigma).

RNA-seq and RRBS data analysis

RNA sequencing was performed for 7 samples: 3 *Sdhb*-/-, 2 *Sdhd*-/- and 2 WT imCC. Enriched samples were used to generate sequencing libraries with the Illumina 'TruSeq Stranded mRNA Sample Prep' kit and associated protocol provided by the manufacturer. Libraries were sequenced by IntegraGen (Evry, France) on an Illumina HiSeq 2000 as paired-end 75 bp reads. Reduced Representation Bisulfite Sequencing (RRBS) was also performed by Integragen SA, as previously described (17). **Details of the process leading to the evaluation of differential expression and methylation rates are provided in the Supplementary Information**. The sequencing data reported in this paper have been deposited to the EGA (European Genome-phenome Archive) database (European Genome-phenome Archive) database (accession number EGAS00001005279).

Metabolite analysis, high resolution respirometry, enzymatic activities and features of oxidative stress assessment

All cell types underwent metabolite extraction using Methanol:H2O:Chloroform at ratio 1:1:1, following ^{13}C-glucose and ^{13}C-glutamine labeling. The polar fractions were used for Gas Chromatography – Mass Spectrometry (GC-MS) analysis allowing acquisition of the isotope data. High resolution respirometry was performed by loading Intact or permeabilized cells in an Oxygraph-O2 k (Oroboros instruments) chamber, using Mir05 respiratory media and digitonin for the latter. A pseudo dual-wavelength Varian CARY50 spectrophotometer

(Victoria, Australia) was used to assess respiratory chain activities as previously described (23). For the assessment of oxidative stress features, cells treated as stated, were incubated with either CellRox, MitoSox or Bodipy C11 Reagent (Termofisher) and Flow cytometry data were acquired using an LSR FORTESSA analyzer (BD biosciences).

Cellular and tumoral iron and copper analysis

For cellular iron and copper assessment, cells were incubated with the relevant metal-specific probe prior to being analyzed by flow cytometry on a BD Accuri C6 (BD Biosciences). Laser ablation-inductively coupled plasma-mass spectrometry (LA-ICP-MS) was performed on dewaxed and rehydrated formalin-fixed paraffin-embedded tumor sections. **Details of LA-ICP-MS experiments are provided in the Supplementary Information**. LA-ICP-MS images were acquired in a fixed dosage mode, with a vertical and horizontal spatial resolution of 20 μm, a detailed list of sample settings is available in Supplementary Table 1. Average ^{56}Fe and ^{63}Cu intensities were calculated from pixels containing a positive elemental tissue marker (^{31}P) ensuring background regions did not influence these calculations.

qRT-PCR, Western-blot, immunofluorescence staining and immunohistochemical analyses

For qRT-PCR, total mRNA was extracted from cell pellets using RNeasy plus mini-kit (Qiagen). Reverse transcription was fulfilled using iScript™ cDNA Synthesis Kit (BIO-RAD) and qRT-PCR was performed on CFX96™ Real-Time System C1000 Touch™ Thermal Cycler (BIO-RAD) using SuperScript SybrGreen (BioRad) to assess the expression of *Sdhb*, *Sdhd*, *Snai1*, *Fn1*, *Epas1*, *MMP9* and *18S*. Western-blot analysis were performed to assess SDHB, SDHA, HIF2α and TUBULIN expression. RIPA lysis buffer was used for extraction of total protein and concentrations were determined with Bradford colorimetric method. Results were read with a LAS-4000 Mini (Fuji). Actin staining and γH2AX immunofluorescence were performed on cells plated on glass slides, while γH2AX immunohistochemistry was performed on 6 μm sections from paraffin-embedded tumors. **Details of primers, primary and secondary antibodies, immunostaining, and experimental conditions are provided in the Supplementary Information**.

Data analysis

Data are represented as mean (of at least 3 independent experiments) ± SEM (standard error of the mean). Data were analyzed by one-way or 2-way ANOVA. Statistics tests were carried out using the GraphPad Prism software. All analyses considered a value of $P \leq 0.05$ to be statistically significant. For enrichment analysis, we used an in-house adaptation of the GSEA method to identify gene sets from the MSigDB database overrepresented among up/down-regulated and hyper/hypomethylated genes.

Results

Loss of SDHB or SDHD leads to similar metabolic dysfunction and respiratory profiles

To investigate the mechanisms underlying the metastatic characteristics of *SDHB* mutated-PPGL but not of *SDHD*-deficient tumors, we knocked-out the *Sdhd* gene using the CRISPR/Cas9 procedure in wild-type (WT) imCC (17). We obtained two independent *Sdhd*-/- clones

(ClA and ClB) each containing a different homozygous point mutation on exon 3 of *Sdhd*, c.119delC and c.120_121delCA, respectively, both leading to premature stop codons (Fig. 1A). These mutations were predicted to lead to the translation of truncated proteins of 79 and 68 amino acids, respectively, instead of the 159 amino acids of the entire WT SDHD protein. To attest for the absence of off-target effects in *Sdhd-/-* cells, we generated a third cell line, in which SDHD loss was rescued by stably transfecting an *Sdhd*-expressing vector in the *Sdhd*-/- ClA (clone *Sdhd-R*). *Sdhd*-mutated cells showed a decrease in *Sdhd* RNA levels (Supplementary Fig. 1A) when compared with WT and *Sdhd-R* cells, which may be suggestive of nonsense-mediated decay in the mutant clones, and particularly in clone A.

SDHD protein expression could not be estimated due to the lack of efficient antibody in mouse. It is worth noting that *Sdhd* mRNA levels were also reduced in *Sdhb*-deficient cells. In contrast, *Sdhb* mRNA levels were absent in *Sdhb-/-* cells, but not significantly reduced in *Sdhd-/-* imCC (Supplementary Fig. 1B). It has previously been reported that disassembly of the SDH complex in case of *SDHx* mutations leads to the degradation of the SDHB subunit in all *SDHx* mutant cells (24). However, our data show that *Sdhd-/-* clones retain a small but significant level of SDHB protein (Fig. 1B). Similarly, evaluation of SDHB protein by immunohistochemistry in SDH-related PPGL frequently leads to a weak diffuse signal in SDHD deficient tumors, while it is totally negative in SDHB-mutated ones, suggesting that some SDHB remains present in this type of mutants (25). Nevertheless, they exhibited a complete loss of SDH enzymatic activity, similar to that observed in *Sdhb*-deficient cells (Fig. 1C), and in accordance with observations in mutated human PPGL (9,26). Interestingly, it has previously been suggested that succinate accumulation might be less important in SDHD-deficient tumors, which may account for their different metastatic potential (27). Analysis of intracellular succinate levels revealed a substantial accumulation of succinate in *Sdhd-/-* cells that reached that observed in the $Sdhb^{-/-}$ imCC model (Fig. 1D). Similarly, levels of the related metabolites, fumarate and 2-oxoglutarate, were strongly reduced in all SDH-deficient cells regardless of the subunit inactivated. *Sdhd-R* cells showed a profile similar to that of WT imCC (Fig. 1E-F and Supplementary Fig. 1C, D).

Next, we assessed the metabolic and respiratory phenotypes of both types of SDH-deficient cells. ^{13}C-glucose tracing experiments revealed that in accordance with previous work (21), cells deficient in SDH-activity undergo a metabolic rewiring in the absence of a fully functional TCA cycle (Fig. 2A). Like *Sdhb-/-* cells, the synthesis of aspartate by *Sdhd-/-* imCC cannot rely on oxidative TCA cycle metabolism (Fig. 2B and C, m+2 isotopomer) and instead increase the aspartate produced through pyruvate carboxylation (PC) (Fig. 2B and C, m+3 isotopomer) for anabolic purposes. Equally, their synthesis of citrate from glucose, a central metabolite for cellular anabolism, was greatly reduced (Fig. 2B). The metabolism of another key nutrient, glutamine was therefore examined. Although both cell lines retain some oxidative metabolism of glutamine to produce succinate, *Sdhd-/-* imCC appear to significantly increase their synthesis of aspartate and citrate using reductive carboxylation (Fig. 2C and D), which is not observed to the same degree in *Sdhb-/-* imCC. We then measured oxygen consumption of intact and permeabilized imCC (Fig.2E and F). In both cases, *Sdhb-/-* imCC exhibited no significant change in basal respiration, while *Sdhd-/-* cells showed a decrease, suggesting that a more significant defect in respiration exists in the *Sdhd-/-* cells compared to *Sdhb-/-*. Maximal respiratory capacity (FCCP-mediated

uncoupled respiration) was significantly reduced in both SDH-deficient imCC models, in compliance to that previously reported in *Sdhb-/-* cells(28). The relative decrease in respiratory activity observed in *Sdhd-/-* cells compared to those deficient in *Sdhb* was consistent with the increased reliance on reductive carboxylation for the synthesis of aspartate and citrate (Fig. 2C), an effect previously observed in hypoxia (29). Given the decreased oxygen consumption observed in the *Sdhd*-deficient cells compared to those lacking *Sdhb*, we examined whether there was a compensatory increase in pyruvate reduction to lactate to regenerate cytosolic NADH and maintain glycolysis. We indeed saw that while *Sdhb-/-* cells show a small increase in lactate production, this is further increased in *Sdhd*-deficient cells (Fig. 2G).

Altogether, these results suggest that massive succinate accumulation and rewired metabolism do not constitute relevant triggers for SDHB-related malignancy, although the extent of mitochondrial respiratory deficit may vary between the two models.

Sdhb knockout in mouse chromaffin cells promotes neuroendocrine-to-mesenchymal transition (NMT), unlike Sdhd knockout

We previously reported that *Sdhb-/-* imCC exhibit a mesenchymal-like phenotype with increased adhesion, migration and invasion capacities (19). Morphological observation following phalloidin staining qualitatively revealed that *Sdhd-/-* cells appear to be generally smaller than *Sdhb-/-* cells, and display a less extensive and rather peripheral actin mesh unlike *Sdhb-/-* imCC (Fig. 3A), suggesting that only *Sdhb-/-* cells undergo mesenchymal transformation. Accordingly, markers of NMT activation such as *Snai1*, *Mmp9, Fn1* (Fig. 3B) were overexpressed in *Sdhb-/-* imCC but not in *Sdhd-/-* cells. In accordance with the loss of neuroendocrine features, *NCadh* was downregulated in *Sdhb-/-* imCC, while it was actually overexpressed in *Sdhd-/-* cells (Supplementary Fig. 2A). *Sdhd-/-* cells showed moderate increase in adhesion (Fig. 3C), and no increase in migration, evaluated both in collective (Fig. 3D) and individual migration assays (Supplementary Fig. 2B). *Sdhd-/-* imCC also exhibited a much slower cell growth than *Sdhb-/-* cells (Supplementary Fig. 2C). Hence, despite similar SDH loss-of-function and succinate levels, *Sdhd*-deficient cells do not display the mesenchymal and migratory phenotype of *Sdhb* KO cells, as observed in human paraganglioma(18).

Sdhb-deficient cells show greater inhibition of 2OG-dependent dioxygenases

We have previously established that *SDHB*-mutated PPGL and *Sdhb-/-* imCC display pseudohypoxic and hypermethylator phenotypes, caused by inhibition of PHD and TET enzymes and involved in the mesenchymal-like hallmarks associated with SDHB deficiency (17,20). We next performed reduced representation bisulfite sequencing (RRBS) to precisely quantify 5-methyl-cystosine (5mC) modifications along the genome after enrichment for CpG rich regions in the different cell lines. Compared to WT, both *Sdhb* and *Sdhd* KO cells displayed a DNA hypermethylator phenotype, but this phenotype was less pronounced in *Sdhd*-/- cells (Fig. 3E). In total, *Sdhb-/-* cells displayed 6,847 significantly hypermethylated gene-based features (TSS +/- 500 bp and gene bodies) against only 2,564 for *Sdhd*-/- cells (Fig. 3F and Supplementary Table 2). Hypermethylator phenotypes in *Sdhb*-/- and *Sdhd*-/- cells displayed a significant overlap and correlation (Fig. 3G and H), with 1,084 common

hypermethylated features representing 42% and 16% of hypermethylated features in *Sdhd*-/- and *Sdhb*-/- imCC, respectively.

Surprisingly, Western-blot analysis in our cell lines revealed stabilization and massive increase of HIF2α protein levels in *Sdhb-/-* cells, which was not seen in either *Sdhd-/-,* WT or *Sdhd*-R imCC (Fig. 3I). We thus analyzed the transcriptome of all cell lines using RNA-sequencing. Hierarchical clustering of expression profiles across the 1,000 most variant genes (based on standard deviation) showed that *Sdhd*-/- imCC remain closer to wild-type cells and display less gene expression changes than *Sdhb*-/- cells (Fig. 3J). To investigate more specifically the expression of hypoxia-inducible genes, we analyzed the expression of a previously published list of 52 HIF targets (3), among which 47 were present in the transcriptome of imCCs (Supplementary Table 3). Twenty-four (24) of them were overexpressed in Sdhb-deficient cells compared to WT (mean value >120% of WT), while 17 were overexpressed in Sdhd-deficient cells compared to WT (13 overlapping with those high in Sdhb KO cells) (Fig. 3K). Comparison of both KO cells showed that 19 of the 28 overexpressed genes showed stronger expression in *Sdhb-/-* cells (Fig. 3L). These data therefore suggested that although HIF2α was hardly detectable by western blot, *Sdhd-/-* cells did show a mild pseudohypoxic signature. In order to validate this observation, we further analyzed previously-published transcriptome data generated in a collection of 188 human PPGL. In this study, 3 *SDHD,* 1 *SDHA* and 2 *SDHC*-mutated PPGL were evaluated together with 17 *SDHB*-mutated ones (3), which all clustered together using the expression of the 52 HIF-target genes. We have reanalyzed these data, limiting them to the 41 highly expressed ones, and we evaluated their mean expression in *SDHB* versus *SDHD*-mutated tumors. We observed that most genes were overexpressed in SDHB-related tumors while the subset of genes over-represented in *SDHD*-mutated tumors corresponded to genes expressed by endothelial cells or associated with angiogenic processes (Supplementary Fig. 3A), therefore reflecting the very high vascular density described in these tumors (15,30). Similar results were obtained on the TCGA cohort of PPGL (Supplementary Fig. 3B)(31).

Altogether, these findings indicate that *Sdhd* inactivation induces less DNA methylation and gene expression changes than *Sdhb* deletion. We next aimed at identifying the causes of the seemingly greater inhibition of 2OG-dependent dioxygenases in *Sdhb-/-* cells.

Iron and copper homeostasis are dysregulated in SDH-deficient cells, and especially in Sdhb KO cells

2OG-dependent dioxygenases are iron-containing enzymes. Because SDHB is the iron-sulfur subunit of complex II, we wondered whether its complete loss might lead to disturbances in iron metabolism, which would in turn modulate the activity of 2OG-dependent dioxygenases. We thus used specific fluorescent probes to detect cytosolic and mitochondrial iron in all cell types, as well as assessed iron levels in tumor samples from patients with *SDHB* mutations. We also evaluated mitochondrial copper in all cell types. Indeed, iron and copper are both essential metals with close metabolic interactions that have been known for a long time (32).

We first used the commercial Calcein-AM probe that reveals both Iron(II) and Iron(III) levels, but also other ions such as calcium. This experiment showed a decrease in global

labile iron in SDH-deficient cells compared to WT imCC (Fig. 4A). To validate this observation in human PPGL, we performed laser ablation-inductively coupled plasma-mass spectrometry (LA-ICP-MS) in 6 pheochromocytomas carrying *NF1* (n=2), *RET* (n=2) or *SDHB* (n=2) mutations, as well as 4 paragangliomas with *SDHB* (n=2) or *SDHD* (n=2) gene mutations. We observed that average ^{56}Fe counts were significantly decreased in tumors with *SDHB* mutations compared with tumors with *NF1*, *RET* or *SDHD* mutations (Fig. 4B-F). This decrease was greater in *SDHB*-mutated paragangliomas (Fig. 4D) than in *SDHB*-mutated pheochromocytomas (Fig. 4C). These results obtained in tumors from patients consolidate the hypothesis that loss of the SDHB subunit leads to an altered iron metabolism. Calcein-AM probe being poorly specific, we next examined the subcellular localization of Iron(II) using specific probes of both this ion, and specific cell compartments. Unexpectedly, evaluation of the labile pool of cytosolic Iron(II) revealed a significant increase in *Sdhb-/-* cells only (Fig. 4G). This suggests that the calcein-AM data would actually be imputable to a strong decrease in cytosolic levels of Iron(III) in SDH-deficient cells. In opposition, we observed a significant decrease in the mitochondrial pool of chelatable iron (Iron(II)) in both knockout models, decrease which was especially pronounced in *Sdhb-/-* cells and rescued in *Sdhd-R* imCC (Fig. 4H).

We next evaluated mitochondrial copper levels in all cell types. Concerning the pool of labile mitochondrial Cu(II), no significant changes were observed in the SDH-deficient cells, while mitochondrial Cu(I) was significantly increased in *Sdhb* KO cells only (Supplementary Fig. 4A and B). LA-ICP-MS was also used to quantify the levels of ^{63}Cu in 10 PPGL tumors. This evaluation of global copper was not able to confirm the difference in *SDHB vs RET* or *NF1* tumors. However, it suggested that SDHD-deficient PGL had a decrease in copper counts compared with the other genotypes (Supplementary Fig. 4C). Hence, there was a dysregulation in copper and especially in iron pools in cells and tumors depending on their genotypes. In support of these observations, we evaluated the mRNA expression of several iron and copper transporters as well as of chaperones or different actors of iron/copper homeostasis, which revealed that these pathways were indeed strongly affected in *Sdhb* KO cells (Fig. 4I, J). In particular, these cells showed a differential expression of transporters implicated in the entry of iron and copper in the cell and the mitochondria: high DMT1 (*Slc11a2*) and low Slc25a37 would sustain the increased cytosolic distribution of Iron(II), while low CTR1 (*Slc31a1*) and high Slc25a3, the high mitochondrial Cu(I) levels. Consistently with these observations, human PPGL transcriptome data showed an increase in *DMT1* mRNA levels in SDH tumors as compared with other types of mutated PPGL. SDH tumors also exhibited a slight increase in the expression of other actors involved in iron binding and transport, such as the hypoxia-inducible genes *TF* and *TFRC*. *SLC31A1* was significantly decreased in both SDH and VHL tumors compared to RET or NF1-mutated ones. No differences were detected for *TFR2* nor *SLC25A3* expression (Supplementary Fig. 4D).

Sdhb-deficient cells display increased ROS levels without activation of the NRF2 pathway

Sdhb-KO cells show increased mitochondrial copper(I) and cytosolic Iron(II) levels, which could cause important oxidative stress in these cell compartments (33). An increase in reactive oxygen species (ROS) might also participate to the sustained inhibition of 2OG-

dependent dioxygenases activity (34). Flow cytometry analyses of fluorescent probes revealed that *Sdhb*-deficient cells showed increased ROS both in the cytosol (Fig. 5A) and especially in the mitochondria (Fig. 5B). They also displayed a significant increase in lipid peroxidation levels (Fig. 5C) and in mitochondrial activity (Fig. 5D) but not in overall mitochondrial mass (Fig. 5E). Unexpectedly, none of the *Sdhd*-deficient clones showed any changes in ROS levels as compared to the WT cells.

Because *Sdhb-/-* cells display such a significant increase in ROS, we postulated that they would probably show increased anti-oxidant responses, either through superoxide dismutase (SOD) or through activation of the NRF2 pathway. However, the global superoxide dismutase activity did not differ between the different cell types (Supplementary Fig. 5A). Moreover, RNA-seq analysis showed a significant downregulation of mitochondrial SOD2, thus demonstrating that *Sdhb*-deficient cells do not detoxify the excess in mitochondrial ROS (Fig. 5F).

We performed gene set enrichment analyses using RNA-seq data of 58 NRF2-target genes (Supplementary Table 4) which showed no activation of the pathway in *Sdhb* nor in *Sdhd* KO cells, compared to WT (Supplementary Fig. 5B). In addition, treating the cells with N-acetyl cysteine (NAC) had no effect on the levels of mitochondrial ROS in any of the cell types studied (Fig. 5G), neither affected their proliferation (Fig. 5H). In order to fully validate this observation in the human context, this list of genes was also tested in the transcriptome data of the human PPGL COMETE collection (Fig. 5I). Mean values of NRF2 targets levels in the groups of sporadic non-mutated tumors (n=49), *RET* (n=19), *NF1* (n=37), *VHL* (n=40), *SDHA, C, D-* (n=6) and *SDHB*-mutated tumors (n=17) were used to perform unsupervised classification, which confirmed that the NRF2 pathway is not activated in *SDHB*-deficient tumors.

It has previously been reported that SDHB loss is associated with increased DNA damage (35), and a sensitivity to inhibitors of poly (ADP-ribose) polymerase (PARP) (35, 36, 37). In addition to the recently demonstrated mechanism associated with oncometabolite-induced inhibition of the lysine demethylase KDM4B, increased ROS levels may participate to such phenotype. We therefore evaluated DNA damage after staining PPGL tumor tissues and imCCs with anti-γH2AX antibody (Supplementary Fig. 5C and D). Although it was not statistically significant, we observed a slight increase in γH2AX levels in SDHB-deficient tumors, which was not seen in *Sdhb-/-* imCCs. Treating cells with increasing doses of the PARP inhibitor Talazoparib reduced cell survival in all cell types, with an actually higher efficacy in WT and *Sdhd*-R cells (Supplementary Fig. 5E). In this cell model, it seemed that Talazoparib efficiency was not related to SDH-deficiency, but was rather related to cell proliferation indexes of the treated cell types.

Modulating Iron(II) and ROS levels affects pseudohypoxia and survival in Sdhb-deficient cells

Altogether, these data suggest that in *Sdhb* KO cells, a combination of succinate accumulation, dysregulation of iron homeostasis and high ROS levels may account for the increased inhibition of TET and PHD hydroxylases. To demonstrate this link, we treated cells with Iron(II) (50 μM), which had no effect on cytosolic ROS (Supplementary Fig.

6A) but reduced mitochondrial ROS, only in *Sdhb-/-* cells (Fig. 6A). This was associated with a decrease in HIF2α protein levels in *Sdhb-/-* cells as well (Fig. 6B). Treating cells with increasing doses of ferrous iron revealed a specific sensitivity of Sdhb-deficient cells. Indeed, after 48 h of treatment, 0.1 mM doses of Iron(II) led to a 60% decrease in *Sdhb-/-* cells survival while it only moderately affected WT, *Sdhd*-KO or *Sdhd*-R cell types (Fig. 6C).

In order to further demonstrate that increased mitochondrial ROS were indeed responsible for the massive HIF2α stabilization observed in Sdhb-deficient cells, we then treated them for 12h with MitoTEMPO, a mitochondrially targeted antioxidant that acts as a specific scavenger of mitochondrial superoxide. MitoTEMPO (MTT) at 2.5 μM had no effect on cytosolic ROS (Fig. 6D), but significantly decreased mitochondrial ROS in *Sdhb-/-* imCC (Fig. 6E), which was associated with a substantial reduction of HIF2α levels (Fig. 6F). High doses of MTT are suspected to show a reverse effect, promoting a pro-oxidant response. We therefore treated cells with 2.5 mM of the compound and showed that such high dose increased cytosolic ROS in all cell types and especially in WT and *Sdhd-/-* ClA cells (Fig. 6G), as well as mitochondrial ROS in WT and *Sdhb-/-* cells (Fig. 6H). Strikingly, such treatment promoted a strong pseudohypoxic response in WT, *Sdhd-/-* and *Sdhd*-R cells, thus demonstrating that increasing ROS was sufficient to mediate HIF2α stabilization. In contrast, this led to the opposite effect in *Sdhb-/-* cells (Fig. 6I) in which HIF2α protein was almost lost. It actually appeared that high dose MTT was highly toxic for *Sdhb-/-* cells exclusively (Fig. 6J), with perinuclear vacuoles emerging after 12h and leading to the death of all *Sdhb-/-* imCC after 72h.

In an attempt to evaluate another pro-oxidant treatment that might be used in a clinical context, we finally tested the vulnerability of imCC to high dose ascorbate. A dose response curve showed that *Sdhb-/-* cells were indeed much more vulnerable to ascorbate with significant increase in cell death appearing from a 1 mM dose onward, a complete lethality being reached at a 2.5 mM ascorbate dose (Fig. 6K). At the higher dose, 85% of *Sdhb*-deficient cell loss was achieved after 24h, while a similar response was only apparent in *Sdhd* and WT cells after 72h (Fig. 6L). To evaluate the mechanism associated with ascorbate-induced lethality, we measured cytosolic and mitochondrial ROS in cells treated for 48 h with 1 mM ascorbate. At such a dose, there was already a significant lethality of *Sdhb*-KO cells and enough cell material was still available to allow the analyses (Supplementary Fig. 6B). Interestingly, we observed that cytosolic ROS were not modified by ascorbate in any of the cell models (Supplementary Fig. 6C). In contrast, ascorbate led to a massive increase in mitochondrial ROS, specifically in *Sdhb-/-* cells (Fig. 6M).

These data suggest that in *Sdhb*-KO cells ascorbate interacts with the increased Iron(II) labile pool to enhance oxidative stress, leading to rapid cell death.

Discussion

It is well-established that a mutation in the *SDHB* gene is a high risk factor for metastatic PPGL (38) and poor prognosis (6), unlike mutations in other *SDHx* genes (*SDHA*, *SDHC* or *SDHD*) that rarely cause metastatic forms of the disease. This question has been unresolved

for 20 years. Many studies have been performed in the past years, mainly using cell lines exhibiting a decrease or complete lack in the expression of *Sdhb*. Thereby, previous work from our team has shown that metastatic SDHB tumors exhibit a NMT phenotype (18,19), associated with increased DNA methylation in comparison to other *SDHx* mutated tumors (20,39). Further, we have recently demonstrated that this hypermethylated profile is due to TET silencing and that the NMT phenotype observed in *SDHB* mutated tumors is the result of synergistic roles of TET repression and pseudohypoxia, through HIF2 activation (20). Although these data have shed light on some mechanisms undeniably involved in the tumorigenesis of *SDHB* mutated tumors, they do not explain the different clinical outcomes observed in patients carrying mutations in the different *SDHx* genes. In the present study, we were able to characterize and compare two physiologically appropriate cellular models exhibiting a complete knock-out in *Sdhb* or *Sdhd* genes, which strikingly recapitulate most of the phenotypic characteristics of *SDHB* and *SDHD*-mutated tumors.

Succinate accumulation is probably the major consequence of SDH loss of activity and increased succinate levels in tumor samples are used as a biomarker of SDH-deficiency in PPGL patients (27,40-42). For a long time, it has therefore been considered to be the main trigger of PPGL tumorigenesis. The role of succinate as an oncometabolite was initially demonstrated in 2005, with the demonstration of its inhibiting role on 2OG-dependent PHD enzymes, leading to the subsequent stabilization of HIFα subunits even under normoxia (43,44). Later, it was demonstrated that succinate is also a major epigenetic modifier, inhibiting TET enzymes and promoting a genome wide hypermethylated profile (17,39,45). It has been suggested that a stronger inhibition of 2OG-dependent dioxygenases observed in *SDHB*-mutated tumors versus tumors with mutations in other *SDHx* genes, might be explained by a fuller inactivation of SDH enzyme associated with higher succinate (27). Here, we firmly invalidate this long-held assumption, both *Sdhb-/-* and *Sdhd-/-* imCC models showing the same loss of SDH activity and similar levels of succinate and fumarate (Fig. 1). Indeed, many of the metabolic characteristics investigated were highly similar between the two cell models suggesting that merely measuring overall steady-state succinate and fumarate levels are inadequate for predicting phenotype, and smaller changes in metabolic function may drive downstream. Surprisingly, HIF2α protein was hardly detectable in Sdhd-deficient cells while it was strongly activated in *Sdhb-/-* imCC. This provides further evidence that although aspects of the overall metabolic phenotype were similar between *Sdhb-/-* and *Sdhd-/-* models, as yet unexplored metabolic factors may play a role in the inactivation of the PHD enzymes to stabilize HIF2α. This was unexpected as previous transcriptome analyses of human tumor samples have classified all *SDHx* mutated tumors together with *VHL*-mutated ones in a “pseudohypoxic” cluster (16,17). However, such classifications were based on global transcriptome and obviously included many other pathways. To our knowledge, only three studies have classified PPGL tumors based on the expression of hypoxia-induced genes. Hensen *et al* compared hypoxia-inducible genes in sporadic head and neck PGL (HNPGL) to HNPGL carrying *PGL2* or *SDHD* gene mutations (46). This study was not able to identify any differences in the hypoxic signature of these 3 types of tumors. Besides, Fliedner *et al* evaluated the expression of HIF target genes in a larger collection of *SDHD* (n=14) and *SDHB* (n=15) related PPGL and also revealed some differences between the two types of tumors, with some genes being less overexpressed

in *SDHD*-mutated PGL (47). Based on previously published transcriptome data (3), our present study shows that most HIF-target genes were overexpressed in SDHB-related tumors while the subset of targets over-represented in *SDHD*-mutated tumors corresponded to genes expressed by endothelial cells. Hence, although it is most probable that, as previously suggested in other studies (15,48-50), *SDHD* tumors display some induction of pseudo-hypoxia *in vivo*, the combination of our *in vitro* data and human PPGL studies does suggest that this effect is at least much more limited in non-*SDHB* mutated cells and can therefore not be imputable to succinate accumulation only.

Our data reveal that while SDHB expression is completely abolished in *Sdhb-/-* cells, a small fraction of SDHB protein remains detectable in *Sdhd-/-* clones, consistently with IHC data on tumors that frequently report a weak diffuse SDHB staining in SDHD-mutated PPGL (25,51). SDHB is the Fe-S subunit of Complex II and contains two highly conserved L(I)YR motifs that are essential for acquisition of Fe-S clusters by recruiting the Fe-S transfer machinery. We postulate that the loss in mitochondrial Fe-S clusters present in the SDHB subunit, may be responsible for the significant imbalance in cytosolic and mitochondrial iron distribution, that we observe in *Sdhb-/-* cells. Interestingly, Saxena et al reported that 37% of disease-causing missense mutations in SDHB were located in either the L(I)YR Fe-S transfer motifs or in the 11 Fe-S cluster-ligating cysteines. Moreover, analyses of reported missense mutations in patients with SDH-RCC or GIST revealed that 50% of these patients had *SDHB* mutations in the L(I)YR motif amino acid residues (52). Altogether, these observations point to a central role of Fe-S clusters loss in SDHB-related disease, which are further reinforced by our present observations.

This labile iron overload may in turn be responsible for or exacerbate the overproduction of ROS observed in *Sdhb-/-* cells, thereby indirectly activating pseudohypoxia and DNA methylation. Indeed, it has been previously demonstrated in a number of studies that in the context of excessive ROS levels, these oxidant molecules can act as signals able to trigger the stabilization of HIFα transcription factors in normoxic conditions (53-55; 34). Besides, in the present study we show that the use of MitoTEMPO, a mitochondrially targeted antioxidant at low concentrations led to a significant decrease in mitochondrial ROS, resulting in turn in reduced HIF2α levels. Conversely, high doses of MTT appear to exert a pro-oxidant action leading to increased cytosolic ROS in all of the cell types, resulting in a strong pseudohypoxic response. Altogether, these results demonstrate the direct link between ROS and HIF2α stabilization and suggest that the elevated ROS levels observed in *Sdhb-/-* cells are probably responsible for their stronger pseudohypoxic phenotype. The association between SDH-deficiency and ROS production has been controversial, with some studies showing an increase in ROS levels (28,53) and others not (56). Actually, these apparently contradictory data are in total accordance with our observations. Indeed, Selak *et al* first reported the absence of oxidative stress following SDH inactivation, but this was observed in an *SDHD* KD cell model (56). In contrast, Guzy et al. proposed that the mechanism explaining PPGL tumorigenesis following SDH inhibition was an increase in ROS production, acting as messengers able to activate pseudohypoxic responses and probably resulting in oxidative damage to DNA, genomic instability, and tumorigenesis (53). In that study, an *Sdhb*-Knock Down (KD) model was compared to a *Sdha*-KD one, and ROS increase was only observed in *Sdhb* KD cells. At that time, it was suspected that *SDHA* gene

mutations were not associated with PPGL, an assumption that we demonstrated to be untrue several years later (3). Based on these observations, their conclusions were that loss of all but the SDHA subunits of SDH would produce such increase in ROS production, explaining SDHB/C/D-mediated tumorigenesis. In view of the actual knowledge on SDH genetics, the combination of these data with our current observations suggests that ROS production is a specific feature of *SDHB*-mutated cells, and may be responsible, not for SDH-related tumorigenesis in general, but for SDHB-related aggressive phenotype.

Our data suggest that the increased oxidative stress observed in *Sdhb*-deficient cells could be the consequence of the dysregulated iron/copper homeostasis. Indeed, redox-active iron strongly interacts with hydrogen peroxide through the Fenton/Haber-Weiss reaction. This usually slow reaction is catalyzed by labile iron, yielding mainly the highly reactive and toxic hydroxyl radical (•OH) from hydrogen peroxide (H_2O_2) and superoxide ions ($•O_2^-$): Iron(III) + $•O_2^-$ → Iron(II) + O_2 ; Iron(II) + H_2O_2 → Iron(III) + OH^- + •OH (57). Oxidative damage arising from excessive levels of ROS are observed in a variety of pathologies such as neurodegenerative diseases and cancer, and have been linked to malignant transformation, together with an imbalance in iron homeostasis(58). Similar assumptions can be made for copper (59). Our results are also consistent with a recent study demonstrating the role of histone H3-H4 as a copper reductase enzyme that binds Cu(II) and catalyzes its reduction to Cu(I). They showed that active H3-H4 is required for proper utilization of copper for mitochondrial respiration and SOD function. Thereby, the excess of mitochondrial Cu(I) observed here predominantly in *Sdhb-/-* imCC suggests a greater inactivation of H3-H4 and thereby may explain the inhibition of *Sod2* expression and the mitochondrial respiratory deficit observed following Sdhb-deficiency (60). In addition, the lack of ROS changes observed in *Sdhd* KO cells might be associated with a residual activity of Complex II in *Sdhb* KO cells. Indeed, while changes in SDH activity coupled to complexes I and III have been shown in a number of different systems to generate ROS, SDH itself has also been suggested to generate ROS when electron flow is compromised (61). It was recently suggested that cells lacking SDHB maintain some form of SDH subunit-containing complex (62), which maintains some level of activity. Although we have no data to validate this hypothesis, one could hypothesize that SDHB-deficient cells can generate ROS due to the retention of an ‘SDH-like’ complex, while SDHD-deficient cells avoid this through complete loss of SDH.

In this regard, our findings are consistent, although different, with those recently proposed by Liu *et al* (63). Using an *Sdhb* KD cell model, these authors also describe ROS accumulation associated with an increase in the intracellular labile iron pool. Surprisingly, these authors observed an increase in iron pool using the calcein probe while in our model, and in human PPGL, this experiment actually showed a decrease in *Sdhb* KO cells. A possible explanation stands in the fact that the model used in the current study is, as the human PPGL studied, a true genetic KO with no SDHB expression, while the model used by Liu *et al* is a KD in which 30% of SDHB protein expression remains. Hence, these different models point to similar pathways, but with major differences in the adaptive responses of the cells. Indeed, Liu *et al* propose that the iron overload would be due to increased expression of TF and TFR2, while, as previously mentioned such overexpression was not observed in our model. We did observe a slight increase in TF mRNA levels in SDH tumors as

compared with other types of mutated PPGL, but not in TFR2. However, in both cases, levels of expression were actually extremely low in all PPGLs and therefore probably not biologically relevant (Supplementary Fig. 4). Furthermore, these authors showed in the same model, that anti-oxidant responses were increased following *SDHB* KD, notably through the upregulation of the nuclear factor erythroid 2-related factor 2 (NRF2). We did not observe any activation of neither the NRF2 pathway nor superoxide dismutase (SOD) activity in any of our different cell types and these data were further validated by our analysis of the transcriptome of human PPGL. Besides, N-acetyl cysteine (NAC) treatment, an inhibitor of the NRF2 pathway, had no effect on the production of mitochondrial ROS by *Sdhb-/-* cells. Hence, it is quite interesting to notice that although similar pathways seem to be affected in the *Sdhb* KO and KD cells (i.e. iron homeostasis, oxidative stress), it seems that the mechanisms and the adaptive responses involved are not similar.

Collectively, these data demonstrate that cells carrying a complete abolition of *Sdhb* gene are not able to neutralize the oxidative damage caused by the mitochondrial ROS excess, through the up-regulation of any intrinsic anti-oxidant pathway. Since, ROS generation seems to be a critical hallmark of SDHB loss, testing an antioxidant treatment that could be used for clinical purposes on our *Sdhb-/-* model appeared relevant. Ascorbate offers many assets, as it presents few side effects in healthy tissues, even at pharmacological concentrations and is easy to access. However, although at physiological concentration (micromolar), ascorbate acts as an antioxidant, able to decrease ROS levels (64), it has been shown to have pro-oxidant actions when reaching high concentrations (65). In addition to its strong oxidative role, ascorbate also affects iron homeostasis, as it reduces ferric iron (Iron(III)) in a cycle of reactions leading to the fully oxidized form of ascorbate (DHA), ferrous iron (Iron(II)) and eventually resulting in increased intracellular ROS levels (66,67). Therefore, in a context of redox imbalance associated with an elevated pool of labile iron, ascorbate treatment could lead to unbearably high ROS levels for the cells and thus aggravate an existing oxidative stress burden. Use of ascorbic acid at pharmacologic concentrations was already suggested as a promising therapeutic strategy on various types of tumor cells exhibiting increased ROS levels, increased labile iron and metabolism impairments (58). All the more that, for the past few years many studies have demonstrated the efficacy of ascorbate as an anticancer treatment, killing cancer cells *in vitro (68,69)* and slowing tumor growth *in vivo* (70). In compliance with these reports, our data reveal that high-dose ascorbate treatment led to a higher accumulation of ROS solely in the mitochondria of *Sdhb-/-* imCC, resulting promptly in cell death, thus validating the increased sensitivity of *Sdhb-/-* cells for ascorbate, mediated by ROS overload. Interestingly, Liu *et al* also recently reported that ascorbate treatment increased apoptosis in *SDHB* KD cells *in vitro* and delayed the growth of tumors as well as of hepatic lesions in xenografted mice models *in vivo* (70). Numerous clinical trials are currently evaluating the efficacy of intravenous high-dose pharmacological ascorbate injection for treating different cancer types (67,71). In that context, ascorbate intravenous injections at pharmacological doses appear as a worthy and highly promising therapeutic strategy to treat SDHB-deficient malignancies, which often exhibit a poor answer to current treatments strategies (radiotherapy, chemotherapy, targeted therapy) and could also be tested in combination with other therapies.

Overall, the comprehensive comparison of the first relevant *Sdhb* and *Sdhd* knock-out cellular models, reveals the common and distinctive pathways used by these cells to adapt to these deficiencies, and highlight specific hallmarks associated with *Sdhb* mutations. Lifting the veil on a long-lasting question, we show that *Sdhb*-deficient cells exhibit stronger PHD and TET inhibition than their *Sdhd*-deficient counterparts, explaining their aggressive phenotype and mesenchymal morphology. We demonstrate that *Sdhb-/-* imCC manifest a significantly exacerbated imbalance in copper and iron homeostasis resulting in an increased labile iron pool, associated with significant ROS accumulation. High-dose ascorbate treatment of *Sdhb-/-* imCC offers promising results, as it highly aggravated the oxidative stress burden endured by *Sdhb*-deficient cells, thus rising as a potential original therapeutic approach to treat malignant PPGL.

Supplementary Material

Refer to Web version on PubMed Central for supplementary material.

Acknowledgements

We thank all members of the Genetics Department, Biological Resources Center and Tumor Bank Platform, Hôpital Européen Georges Pompidou (BB-0033-00063), the Metabolic Tracer Analysis Core (MTAC) at the University of Birmingham for access to their technology platform, as well as the London Metallomics Facility funded by the Wellcome Trust (grant reference 202902/Z/16/Z). We thank Dr Stijn J.M. Van Malderen for assistance with shift correction.

Financial support

This work has received funding from The Plan Cancer, Epigénétique et Cancer (EPIG201303 METABEPIC), The Paradifference Foundation, la Ligue Contre le Cancer (Equipe Labellisée) and the Cancer Research for Personalized Medicine - CARPEM project (Site de Recherche Intégré sur le Cancer - SIRIC). The London Metallomics Facility is funded by the Wellcome trust (grant No 202902/Z/16/Z). Sophie Moog is the recipient of a fellowship from la Fondation pour la Recherche Médicale. Judith Goncalves is the recipient of a fellowship from la Ligue Nationale contre le Cancer. The R.R. research group is funded by the European Research Council (ERC) under the European Union's Horizon 2020 research and innovation programme (grant agreement No [647973]), the Fondation Charles Defforey-Institut de France and Ligue Contre le Cancer (Equipe Labellisée).

References

1. Baysal BE, Ferrell RE, Willett-Brozick JE, Lawrence EC, Myssiorek D, Bosch A, et al. Mutations in SDHD, a mitochondrial complex II gene, in hereditary paraganglioma. Science. 2000; 287: 848–51. [PubMed: 10657297]
2. Astuti D, Latif F, Dallol A, Dahia PL, Douglas F, George E, et al. Gene mutations in the succinate dehydrogenase subunit SDHB cause susceptibility to familial pheochromocytoma and to familial paraganglioma. Am J Hum Genet. 2001; 69: 49–54. DOI: 10.1086/321282 [PubMed: 11404820]
3. Burnichon N, Briere JJ, Libe R, Vescovo L, Riviere J, Tissier F, et al. SDHA is a tumor suppressor gene causing paraganglioma. Hum Mol Genet. 2010; 19: 3011–20. DOI: 10.1093/hmg/ddq206 [PubMed: 20484225]
4. Niemann S, Muller U. Mutations in SDHC cause autosomal dominant paraganglioma, type 3. Nat Genet. 2000; 26: 268–70. [PubMed: 11062460]
5. Pasini B, Stratakis CA. SDH mutations in tumorigenesis and inherited endocrine tumours: lesson from the phaeochromocytoma-paraganglioma syndromes. Journal of internal medicine. 2009; 266: 19–42. DOI: 10.1111/j.1365-2796.2009.02111.x [PubMed: 19522823]
6. Amar L, Baudin E, Burnichon N, Peyrard S, Silvera S, Bertherat J, et al. Succinate dehydrogenase B gene mutations predict survival in patients with malignant pheochromocytomas or paragangliomas. J Clin Endocrinol Metab. 2007; 92: 3822–8. [PubMed: 17652212]

7. Buffet A, Ben Aim L, Leboulleux S, Drui D, Vezzosi D, Libe R, et al. Positive impact of genetic test on the management and outcome of patients with paraganglioma and/or pheochromocytoma. J Clin Endocrinol Metab. 2019. [PubMed: 30698717]
8. Hescot S, Curras-Freixes M, Deutschbein T, van Berkel A, Vezzosi D, Amar L, et al. Prognosis of Malignant Pheochromocytoma and Paraganglioma (MAPP-Prono Study): A European Network for the Study of Adrenal Tumors Retrospective Study. J Clin Endocrinol Metab. 2019; 104: 2367–74. [PubMed: 30715419]
9. Gimenez-Roqueplo AP, Favier J, Rustin P, Mourad JJ, Plouin PF, Corvol P, et al. The R22X mutation of the SDHD gene in hereditary paraganglioma abolishes the enzymatic activity of complex II in the mitochondrial respiratory chain and activates the hypoxia pathway. Am J Hum Genet. 2001; 69: 1186–97. DOI: 10.1086/324413 [PubMed: 11605159]
10. Rao JU, Engelke UF, Sweep FC, Pacak K, Kusters B, Goudswaard AG, et al. Genotype-specific differences in the tumor metabolite profile of pheochromocytoma and paraganglioma using untargeted and targeted metabolomics. J Clin Endocrinol Metab. 2015; 100: E214–22. DOI: 10.1210/jc.2014-2138 [PubMed: 25459911]
11. Morin A, Letouze E, Gimenez-Roqueplo AP, Favier J. Oncometabolites-driven tumorigenesis: From genetics to targeted therapy. Int J Cancer. 2014; 135: 2237–48. [PubMed: 25124653]
12. Müller S, Sindikubwabo F, Cañeque T, Lafon A, Versini A, Lombard B, et al. CD44 regulates epigenetic plasticity by mediating iron endocytosis. Nat Chem. 2020; 12: 929–38. DOI: 10.1038/s41557-020-0513-5 [PubMed: 32747755]
13. Vissers MCM, Kuiper C, Dachs GU. Regulation of the 2-oxoglutarate-dependent dioxygenases and implications for cancer. Biochem Soc Trans. 2014; 42: 945–51. [PubMed: 25109984]
14. Kuiper C, Vissers MCM. Ascorbate as a co-factor for fe- and 2-oxoglutarate dependent dioxygenases: physiological activity in tumor growth and progression. Front Oncol. 2014; 4: 359. doi: 10.3389/fonc.2014.00359 [PubMed: 25540771]
15. Favier J, Briere JJ, Burnichon N, Riviere J, Vescovo L, Benit P, et al. The warburg effect is genetically determined in inherited pheochromocytomas. PloS one. 2009; 4 e7094 doi: 10.1371/journal.pone.0007094 [PubMed: 19763184]
16. Dahia PL, Ross KN, Wright ME, Hayashida CY, Santagata S, Barontini M, et al. A HIF1alpha regulatory loop links hypoxia and mitochondrial signals in pheochromocytomas. PLoS Genet. 2005; 1: 72–80. DOI: 10.1371/journal.pgen.0010008 [PubMed: 16103922]
17. Letouze E, Martinelli C, Loriot C, Burnichon N, Abermil N, Ottolenghi C, et al. SDH Mutations Establish a Hypermethylator Phenotype in Paraganglioma. Cancer Cell. 2013; 23: 739–52. [PubMed: 23707781]
18. Loriot C, Burnichon N, Gadessaud N, Vescovo L, Amar L, Libe R, et al. Epithelial to Mesenchymal Transition Is Activated in Metastatic Pheochromocytomas and Paragangliomas Caused by SDHB Gene Mutations. J Clin Endocrinol Metab. 2012; 97: E954–62. [PubMed: 22492777]
19. Loriot C, Domingues M, Berger A, Menara M, Ruel M, Morin A, et al. Deciphering the molecular basis of invasiveness in Sdhb-deficient cells. Oncotarget. 2015; 6: 32955–65. DOI: 10.18632/oncotarget.5106 [PubMed: 26460615]
20. Morin A, Goncalves J, Moog S, Castro-Vega L-J, Job S, Buffet A, et al. TET-Mediated Hypermethylation Primes SDH-Deficient Cells for HIF2α-Driven Mesenchymal Transition. Cell Rep. 2020; 30: 4551–4566. e7 [PubMed: 32234487]
21. Lussey-Lepoutre C, Hollinshead KE, Ludwig C, Menara M, Morin A, Castro-Vega LJ, et al. Loss of succinate dehydrogenase activity results in dependency on pyruvate carboxylation for cellular anabolism. Nature communications. 2015; 6 8784 doi: 10.1038/ncomms9784 [PubMed: 26522426]
22. n g s in PPGL Study Group. Toledo RA, Burnichon N, Cascon A, Benn DE, Bayley JP, et al. Consensus Statement on next-generation-sequencing-based diagnostic testing of hereditary phaeochromocytomas and paragangliomas. Nat Rev Endocrinol. 2017; 13: 233–47. [PubMed: 27857127]

23. Benit P, Goncalves S, Philippe Dassa E, Briere JJ, Martin G, Rustin P. Three spectrophotometric assays for the measurement of the five respiratory chain complexes in minuscule biological samples. Clin Chim Acta. 2006; 374: 81–6. [PubMed: 16828729]
24. van Nederveen FH, Gaal J, Favier J, Korpershoek E, Oldenburg RA, de Bruyn EM, et al. An immunohistochemical procedure to detect patients with paraganglioma and phaeochromocytoma with germline SDHB, SDHC, or SDHD gene mutations: a retrospective and prospective analysis. Lancet oncol. 2009; doi: 10.1016/S1470-2045(09)70164-0 [PubMed: 19576851]
25. Papathomas TG, Oudijk L, Persu A, Gill AJ, van Nederveen F, Tischler AS, et al. SDHB/SDHA immunohistochemistry in pheochromocytomas and paragangliomas: a multicenter interobserver variation analysis using virtual microscopy: a Multinational Study of the European Network for the Study of Adrenal Tumors (ENS@T). Mod Pathol. 2015. [PubMed: 25720320]
26. Gimenez-Roqueplo AP, Favier J, Rustin P, Rieubland C, Kerlan V, Plouin PF, et al. Functional consequences of a SDHB gene mutation in an apparently sporadic pheochromocytoma. J Clin Endocrinol Metab. 2002; 87: 4771–4. [PubMed: 12364472]
27. Lendvai N, Pawlosky R, Bullova P, Eisenhofer G, Patocs A, Veech RL, et al. Succinate-to-fumarate ratio as a new metabolic marker to detect the presence of SDHB/D-related paraganglioma: initial experimental and ex vivo findings. Endocrinology. 2014; 155: 27–32. DOI: 10.1210/en.2013-1549 [PubMed: 24189137]
28. Kl'učková K, Thakker A, Vettore L, Escribano-Gonzalez C, Hindshaw RL, Tearle JLE, et al. Succinate dehydrogenase deficiency in a chromaffin cell model retains metabolic fitness through the maintenance of mitochondrial NADH oxidoreductase function. FASEB J. 2020; 34: 303–15. [PubMed: 31914648]
29. Metallo CM, Gameiro PA, Bell EL, Mattaini KR, Yang J, Hiller K, et al. Reductive glutamine metabolism by IDH1 mediates lipogenesis under hypoxia. Nature. 2012; 481: 380–4. DOI: 10.1038/nature10602 [PubMed: 22101433]
30. Favier J, Igaz P, Burnichon N, Amar L, Libe R, Badoual C, et al. Rationale for Anti-angiogenic Therapy in Pheochromocytoma and Paraganglioma. Endocr Pathol. 2011. [PubMed: 22183643]
31. Fishbein L, Leshchiner I, Walter V, Danilova L, Robertson AG, Johnson AR, et al. Comprehensive Molecular Characterization of Pheochromocytoma and Paraganglioma. Cancer Cell. 2017; 31: 181–93. DOI: 10.1016/j.ccell.2017.01.001 [PubMed: 28162975]
32. Collins JF, Prohaska JR, Knutson MD. Metabolic crossroads of iron and copper. Nutr Rev. 2010; 68: 133–47. DOI: 10.1111/j.1753-4887.2010.00271.x [PubMed: 20384844]
33. Videla LA, Fernández V, Tapia G, Varela P. Oxidative stress-mediated hepatotoxicity of iron and copper: role of Kupffer cells. Biometals. 2003; 16: 103–11. [PubMed: 12572670]
34. Gerald D, Berra E, Frapart YM, Chan DA, Giaccia AJ, Mansuy D, et al. JunD reduces tumor angiogenesis by protecting cells from oxidative stress. Cell. 2004; 118: 781–94. [PubMed: 15369676]
35. Sulkowski PL, Sundaram RK, Oeck S, Corso CD, Liu Y, Noorbakhsh S, et al. Krebs-cycle-deficient hereditary cancer syndromes are defined by defects in homologous-recombination DNA repair. Nat Genet. 2018; 50: 1086–92. DOI: 10.1038/s41588-018-0170-4 [PubMed: 30013182]
36. Sulkowski PL, Oeck S, Dow J, Economos NG, Mirfakhraie L, Liu Y, et al. Oncometabolites suppress DNA repair by disrupting local chromatin signalling. Nature. 2020; 582: 586–91. DOI: 10.1038/s41586-020-2363-0 [PubMed: 32494005]
37. Pang Y, Lu Y, Caisova V, Liu Y, Bullova P, Huynh T-T, et al. Targeting NAD+/PARP DNA Repair Pathway as a Novel Therapeutic Approach to SDHB-Mutated Cluster I Pheochromocytoma and Paraganglioma. Clin Cancer Res. 2018; 24: 3423–32. DOI: 10.1158/1078-0432.CCR-17-3406 [PubMed: 29636359]
38. Gimenez-Roqueplo AP, Favier J, Rustin P, Rieubland C, Crespin M, Nau V, et al. Mutations in the SDHB gene are associated with extra-adrenal and/or malignant phaeochromocytomas. Cancer Res. 2003; 63: 5615–21. [PubMed: 14500403]
39. Killian JK, Kim SY, Miettinen M, Smith C, Merino M, Tsokos M, et al. Succinate dehydrogenase mutation underlies global epigenomic divergence in gastrointestinal stromal tumor. Cancer Discov. 2013; 3: 648–57. DOI: 10.1158/2159-8290.CD-13-0092 [PubMed: 23550148]

40. Pollard PJ, Briere JJ, Alam NA, Barwell J, Barclay E, Wortham NC, et al. Accumulation of Krebs cycle intermediates and over-expression of HIF1alpha in tumours which result from germline FH and SDH mutations. Hum Mol Genet. 2005; 14: 2231–9. [PubMed: 15987702]
41. Imperiale A, Moussallieh FM, Roche P, Battini S, Cicek AE, Sebag F, et al. Metabolome profiling by HRMAS NMR spectroscopy of pheochromocytomas and paragangliomas detects SDH deficiency: clinical and pathophysiological implications. Neoplasia. 2015; 17: 55–65. DOI: 10.1016/j.neo.2014.10.010 [PubMed: 25622899]
42. Richter S, Peitzsch M, Rapizzi E, Lenders JW, Qin N, de Cubas AA, et al. Krebs cycle metabolite profiling for identification and stratification of pheochromocytomas/paragangliomas due to succinate dehydrogenase deficiency. J Clin Endocrinol Metab. 2014; 99: 3903–11. DOI: 10.1210/jc.2014-2151 [PubMed: 25014000]
43. Selak MA, Armour SM, MacKenzie ED, Boulahbel H, Watson DG, Mansfield KD, et al. Succinate links TCA cycle dysfunction to oncogenesis by inhibiting HIF-alpha prolyl hydroxylase. Cancer Cell. 2005; 7: 77–85. [PubMed: 15652751]
44. Briere JJ, Favier J, Benit P, El Ghouzzi V, Lorenzato A, Rabier D, et al. Mitochondrial succinate is instrumental for HIF1alpha nuclear translocation in SDHA-mutant fibroblasts under normoxic conditions. Hum Mol Genet. 2005; 14: 3263–9. [PubMed: 16195397]
45. Xiao M, Yang H, Xu W, Ma S, Lin H, Zhu H, et al. Inhibition of alpha-KG-dependent histone and DNA demethylases by fumarate and succinate that are accumulated in mutations of FH and SDH tumor suppressors. Genes Dev. 2012; 26: 1326–38. DOI: 10.1101/gad.191056.112 [PubMed: 22677546]
46. Hensen EF, Goeman JJ, Oosting J, Van der Mey AG, Hogendoorn PC, Cremers CW, et al. Similar gene expression profiles of sporadic, PGL2-, and SDHD-linked paragangliomas suggest a common pathway to tumorigenesis. BMC Med Genomics. 2009; 2: 25. doi: 10.1186/1755-8794-2-25 [PubMed: 19432956]
47. Fliedner SMJ, Shankavaram U, Marzouca G, Elkahloun A, Jochmanova I, Daerr R, et al. Hypoxia-Inducible Factor 2α Mutation-Related Paragangliomas Classify as Discrete Pseudohypoxic Subcluster. Neoplasia. 2016; 18: 567–76. DOI: 10.1016/j.neo.2016.07.008 [PubMed: 27659016]
48. Lopez-Jimenez E, Gomez-Lopez G, Leandro-Garcia LJ, Munoz I, Schiavi F, Montero-Conde C, et al. Research resource: Transcriptional profiling reveals different pseudohypoxic signatures in SDHB and VHL-related pheochromocytomas. Mol Endocrinol. 2010; 24: 2382–91. DOI: 10.1210/me.2010-0256 [PubMed: 20980436]
49. Qin N, de Cubas AA, Garcia-Martin R, Richter S, Peitzsch M, Menschikowski M, et al. Opposing effects of HIF1alpha and HIF2alpha on chromaffin cell phenotypic features and tumor cell proliferation: Insights from MYC-associated factor X. Int J Cancer. 2014; 135: 2054–64. [PubMed: 24676840]
50. Welander J, Andreasson A, Juhlin CC, Wiseman RW, Bäckdahl M, Höög A, et al. Rare germline mutations identified by targeted next-generation sequencing of susceptibility genes in pheochromocytoma and paraganglioma. J Clin Endocrinol Metab. 2014; 99: E1352–1360. DOI: 10.1210/jc.2013-4375 [PubMed: 24694336]
51. Santi R, Rapizzi E, Canu L, Ercolino T, Baroni G, Fucci R, et al. Potential Pitfalls of SDH Immunohistochemical Detection in Paragangliomas and Phaeochromocytomas Harbouring Germline SDHx Gene Mutation. Anticancer Res. 2017; 37: 805–12. [PubMed: 28179334]
52. Saxena N, Maio N, Crooks DR, Ricketts CJ, Yang Y, Wei M-H, et al. SDHB-Deficient Cancers: The Role of Mutations That Impair Iron Sulfur Cluster Delivery. J Natl Cancer Inst. 2016; 108. doi: 10.1093/jnci/djv287 [PubMed: 26719882]
53. Guzy RD, Sharma B, Bell E, Chandel NS, Schumacker PT. Loss of the SdhB, but Not the SdhA, subunit of complex II triggers reactive oxygen species-dependent hypoxia-inducible factor activation and tumorigenesis. Mol Cell Biol. 2008; 28: 718–31. DOI: 10.1128/MCB.01338-07 [PubMed: 17967865]
54. Guzy RD, Hoyos B, Robin E, Chen H, Liu L, Mansfield KD, et al. Mitochondrial complex III is required for hypoxia-induced ROS production and cellular oxygen sensing. Cell Metab. 2005; 1: 401–8. [PubMed: 16054089]
55. Mansfield KD, Guzy RD, Pan Y, Young RM, Cash TP, Schumacker PT, et al. Mitochondrial dysfunction resulting from loss of cytochrome c impairs cellular oxygen sensing and hypoxic

HIF-alpha activation. Cell Metab. 2005; 1: 393–9. DOI: 10.1016/j.cmet.2005.05.003 [PubMed: 16054088]

56. Selak MA, Duran RV, Gottlieb E. Redox stress is not essential for the pseudo-hypoxic phenotype of succinate dehydrogenase deficient cells. Biochim Biophys Acta. 2006; 1757: 567–72. [PubMed: 16797480]
57. Torti SV, Torti FM. Iron and cancer: more ore to be mined. Nat Rev Cancer. 2013; 13: 342–55. DOI: 10.1038/nrc3495 [PubMed: 23594855]
58. Schoenfeld JD, Sibenaller ZA, Mapuskar KA, Wagner BA, Cramer-Morales KL, Furqan M, et al. O2.-and H2O2-Mediated Disruption of Fe Metabolism Causes the Differential Susceptibility of NSCLC and GBM Cancer Cells to Pharmacological Ascorbate. Cancer Cell. 2017; 32: 268. [PubMed: 28810149]
59. Ravet K, Pilon M. Copper and iron homeostasis in plants: the challenges of oxidative stress. Antioxid Redox Signal. 2013; 19: 919–32. DOI: 10.1089/ars.2012.5084 [PubMed: 23199018]
60. Attar N, Campos OA, Vogelauer M, Cheng C, Xue Y, Schmollinger S, et al. The histone H3-H4 tetramer is a copper reductase enzyme. Science. 2020; 369: 59–64. DOI: 10.1126/science.aba8740 [PubMed: 32631887]
61. Quinlan CL, Orr AL, Perevoshchikova IV, Treberg JR, Ackrell BA, Brand MD. Mitochondrial complex II can generate reactive oxygen species at high rates in both the forward and reverse reactions. J Biol Chem. 2012; 287: 27255–64. DOI: 10.1074/jbc.M112.374629 [PubMed: 22689576]
62. Bezawork-Geleta A, Wen H, Dong L, Yan B, Vider J, Boukalova S, et al. Alternative assembly of respiratory complex II connects energy stress to metabolic checkpoints. Nat Commun. 2018; 9 2221 doi: 10.1038/s41467-018-04603-z [PubMed: 29880867]
63. Liu Y, Pang Y, Caisova V, Ding J, Yu D, Zhou Y, et al. Targeting NRF2-Governed Glutathione Synthesis for SDHB-Mutated Pheochromocytoma and Paraganglioma. Cancers (Basel). 2020; 12 doi: 10.3390/cancers12020280 [PubMed: 31979226]
64. Buettner GR. The pecking order of free radicals and antioxidants: lipid peroxidation, alpha-tocopherol, and ascorbate. Arch Biochem Biophys. 1993; 300: 535–43. [PubMed: 8434935]
65. Padayatty SJ, Levine M. Vitamin C: the known and the unknown and Goldilocks. Oral Dis. 2016; 22: 463–93. DOI: 10.1111/odi.12446 [PubMed: 26808119]
66. Du J, Cullen JJ, Buettner GR. Ascorbic acid: chemistry, biology and the treatment of cancer. Biochim Biophys Acta. 2012; 1826: 443–57. DOI: 10.1016/j.bbcan.2012.06.003 [PubMed: 22728050]
67. Ngo B, Van Riper JM, Cantley LC, Yun J. Targeting cancer vulnerabilities with high-dose vitamin C. Nat Rev Cancer. 2019; 19: 271–82. DOI: 10.1038/s41568-019-0135-7 [PubMed: 30967651]
68. Chen Q, Espey MG, Krishna MC, Mitchell JB, Corpe CP, Buettner GR, et al. Pharmacologic ascorbic acid concentrations selectively kill cancer cells: action as a pro-drug to deliver hydrogen peroxide to tissues. Proc Natl Acad Sci USA. 2005; 102: 13604–9. DOI: 10.1073/pnas.0506390102 [PubMed: 16157892]
69. Du J, Martin SM, Levine M, Wagner BA, Buettner GR, Wang S, et al. Mechanisms of ascorbate-induced cytotoxicity in pancreatic cancer. Clin Cancer Res. 2010; 16: 509–20. DOI: 10.1158/1078-0432.CCR-09-1713 [PubMed: 20068072]
70. Liu Y, Pang Y, Zhu B, Uher O, Caisova V, Huynh T-T, et al. Therapeutic Targeting of SDHB-Mutated Pheochromocytoma/Paraganglioma with Pharmacologic Ascorbic Acid. Clin Cancer Res. 2020; 26: 3868–80. DOI: 10.1158/1078-0432.CCR-19-2335 [PubMed: 32152203]
71. Nauman G, Gray JC, Parkinson R, Levine M, Paller CJ. Systematic Review of Intravenous Ascorbate in Cancer Clinical Trials. Antioxidants (Basel). 2018; 7 doi: 10.3390/antiox7070089 [PubMed: 30002308]

Europe PMC Funders Author Manuscripts

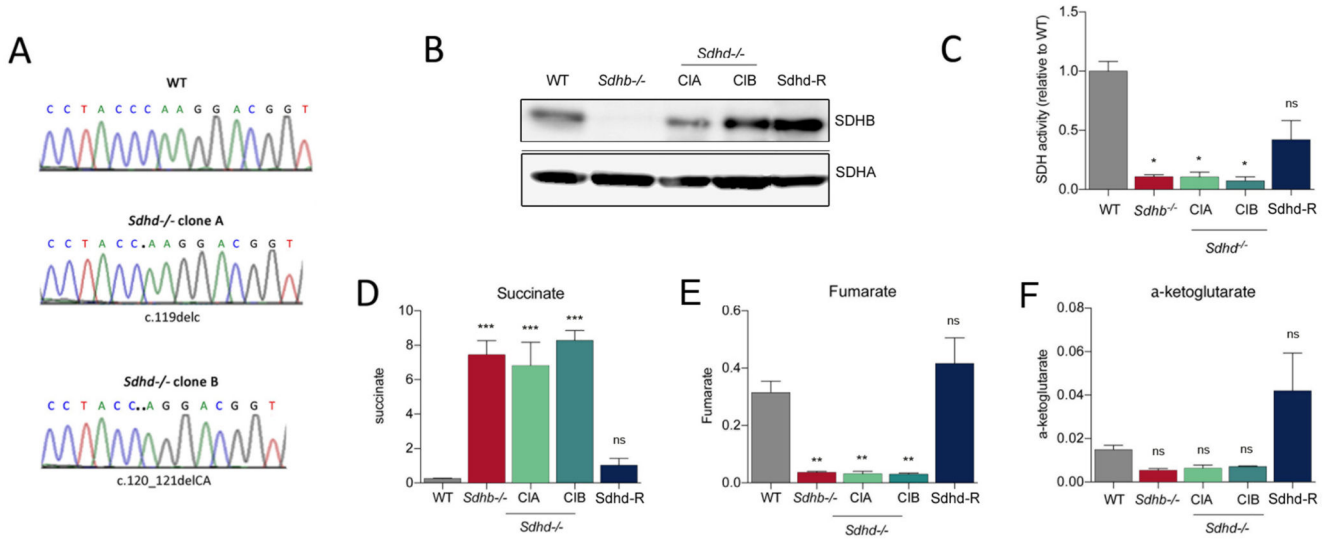

Figure 1. Generation of *Sdhd*-deficient immortalized mouse chromaffin cells.

A, Electrophoregrams of Sanger sequencing of the exon 3 of *Sdhd* gene showing both homozygous point mutations c.119delC and c.120_121delCA of ClA and ClB respectively compared to a control DNA (WT). **B,** Western-blot showing SDHB protein expression in all cell types. **C,** Spectrophotometrical measurement of SDH activity. Steady-state assessment of TCA cycle organic acids (**D,** succinate, **E,** fumarate and **F,** α-ketoglutarate). Results shown are from at least three independent experiments, presented as mean ± SEM. In **C-F**, One-way ANOVA was used to assess statistical significance. ns, not significant, *P≤0.05, **P≤0.01, ***P≤0.001.

Europe PMC Funders Author Manuscripts

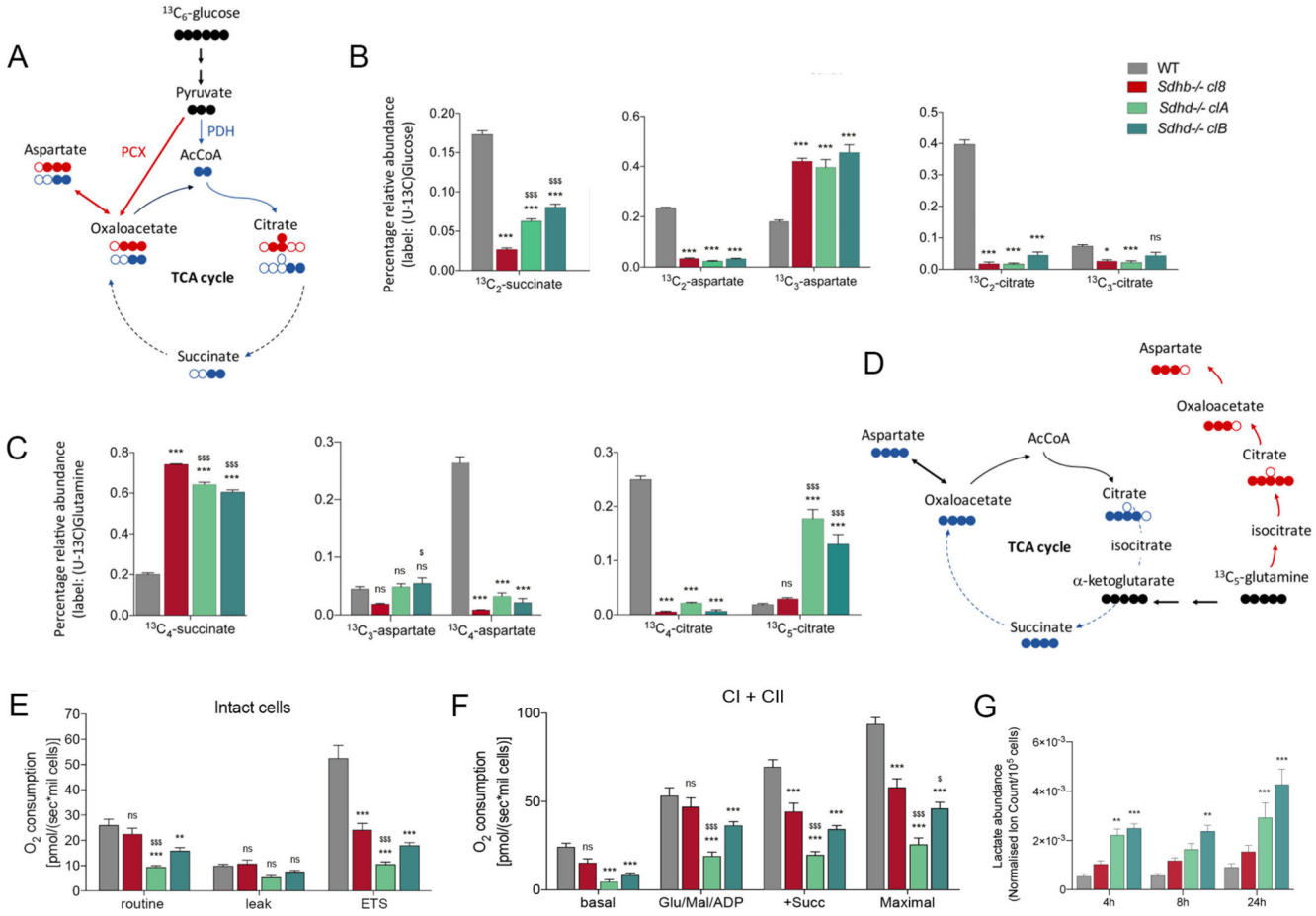

Figure 2. Metabolic and respiratory profiles of *Sdhd*-deficient imCC and *Sdhb-/-* cells.

A, Diagram describing the incorporation of carbons from glucose through PDH (blue) or PCX (red) enzymes activity. Abbreviations in metabolic diagram: PDH, pyruvate dehydrogenase; PCX, pyruvate carboxylase; AcCoA, acetyl coenzyme A. **B,** Incorporation of ^{13}C into succinate, aspartate and citrate in stated cell lines. Isotopomers ^{13}C atoms are shown as filled circles, whereas ^{12}C atoms are empty circles. **C,** Incorporation of $^{13}C_5$-glutamine into succinate, aspartate and citrate in indicated cell lines and **D,** the associated diagrammatic representation of their oxidative (blue) and reductive (red) metabolism. **E,** Oxygen consumption (respiration) of intact and **F,** permeabilized (CI + CII) cells. ETS refers to electron transfer system capacity and basal respiration to oxygen consumption in non-permeabilised cells. **G,** Lactate production over time. Results shown are from at least three independent experiments, presented as mean ± SEM. Two-way ANOVA was performed; ns, not significant, *P≤0.05, **P≤0.01, ***P≤0.001 relative to WT and $P≤0.05, $$$P≤0.001 relative to *Sdhb-/-* imCC.

Europe PMC Funders Author Manuscripts

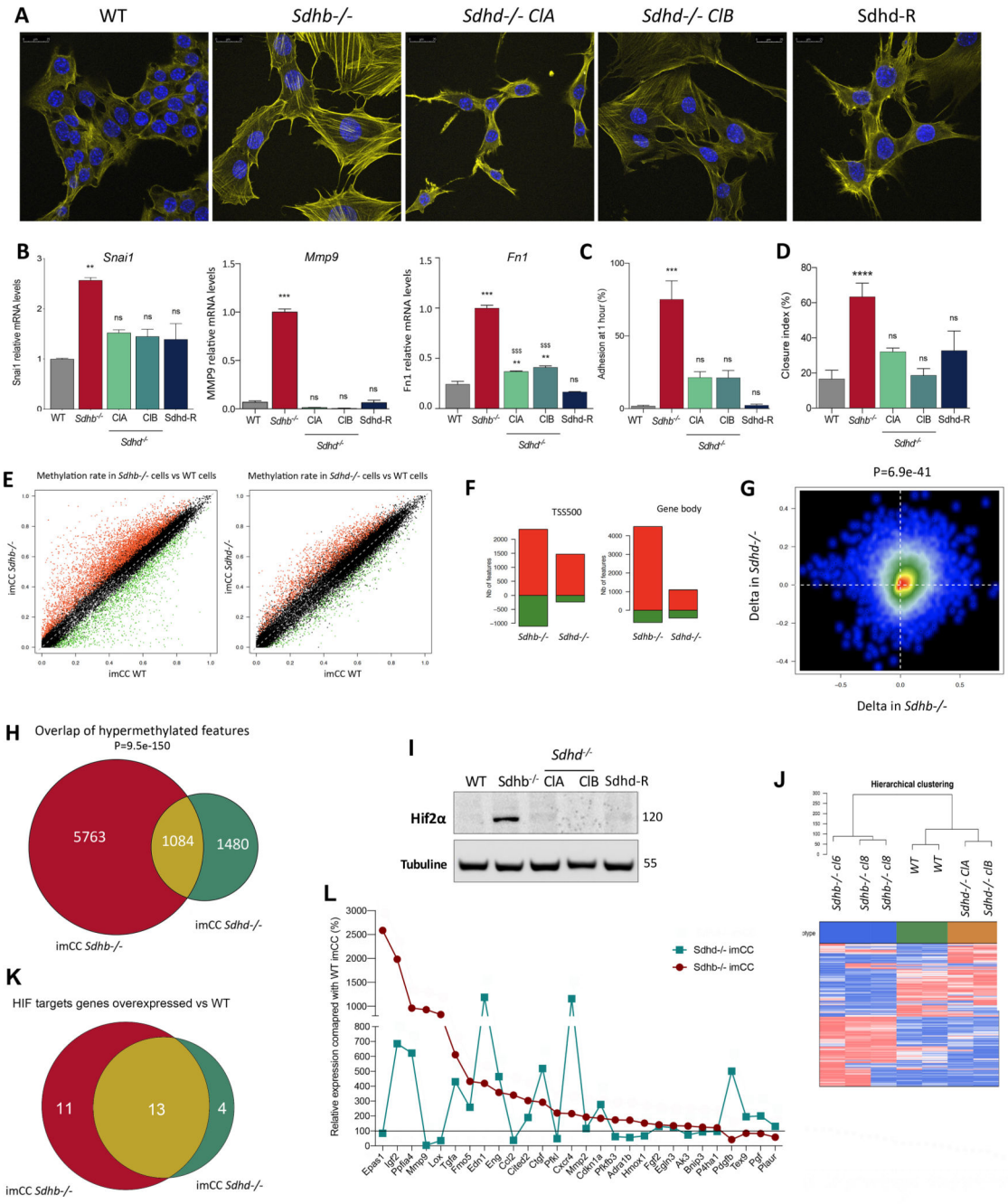

Figure 3. *Sdhb*, but not *Sdhd* knockout in mouse chromaffin cells initiates a mesenchymal phenotype associated with stronger 2OG-dependent dioxygenases inhibition.

A, Actin staining in the indicated cell lines. **B,** qRT-PCR analysis of known epithelial-to-mesenchymal markers (*Snai1*, *Mmp9*, *Fn1*). **C,** Quantification of cell adhesion 1h after plating. **D,** Collective migration assessed after 10h in the stated cell lines, represented as the closure percentage of the wound. **E,** Scatterplot representative of methylation rates identified by RRBS in *Sdhb-/-* versus WT cells and *Sdhd-/-* versus WT cells, respectively. **F,** number of differentially methylated features in *Sdhb-/-* and *Sdhd-/-* imCC (versus WT) in TSS500

and gene body regions. **G,** Comparison of methylation changes generated by *Sdhd* and *Sdhb* knockout in imCC. **H,** Number and overlap of differentially methylated features in *Sdhb-/-* compared with *Sdhd-/-* imCCs. **I,** Western blot of HIF2α in total cellular extracts of indicated cell lines. **J,** Heatmap representation of transcriptome-based classification of imCCs according to their genotype resulting in hierarchical clustering. **K,** Number and overlap of overexpressed hypoxia-inducible genes from a selected list of 47 genes in *Sdhb-/-* and *Sdhd-/-* imCCs compared with WT cells. **L,** Relative expression levels of overexpressed hypoxia-inducible genes in *Sdhb-/-* and *Sdhd-/-* imCCs compared with WT. In **A, B, C, D** and **E** data shown are from at least three independent experiments, presented as mean ± SEM. **K** and **L** data are mean expression levels from RNAseq data generated in 3 *Sdhb-/-,* 2 WT and 2 *Sdhd-/-* clones. One-way ANOVA was used to assess statistical significance; ns, not significant, **P≤0.01, ***P≤0.001 relative to WT and $$$P≤0.001 relative to *Sdhb-/-* imCC.

Europe PMC Funders Author Manuscripts

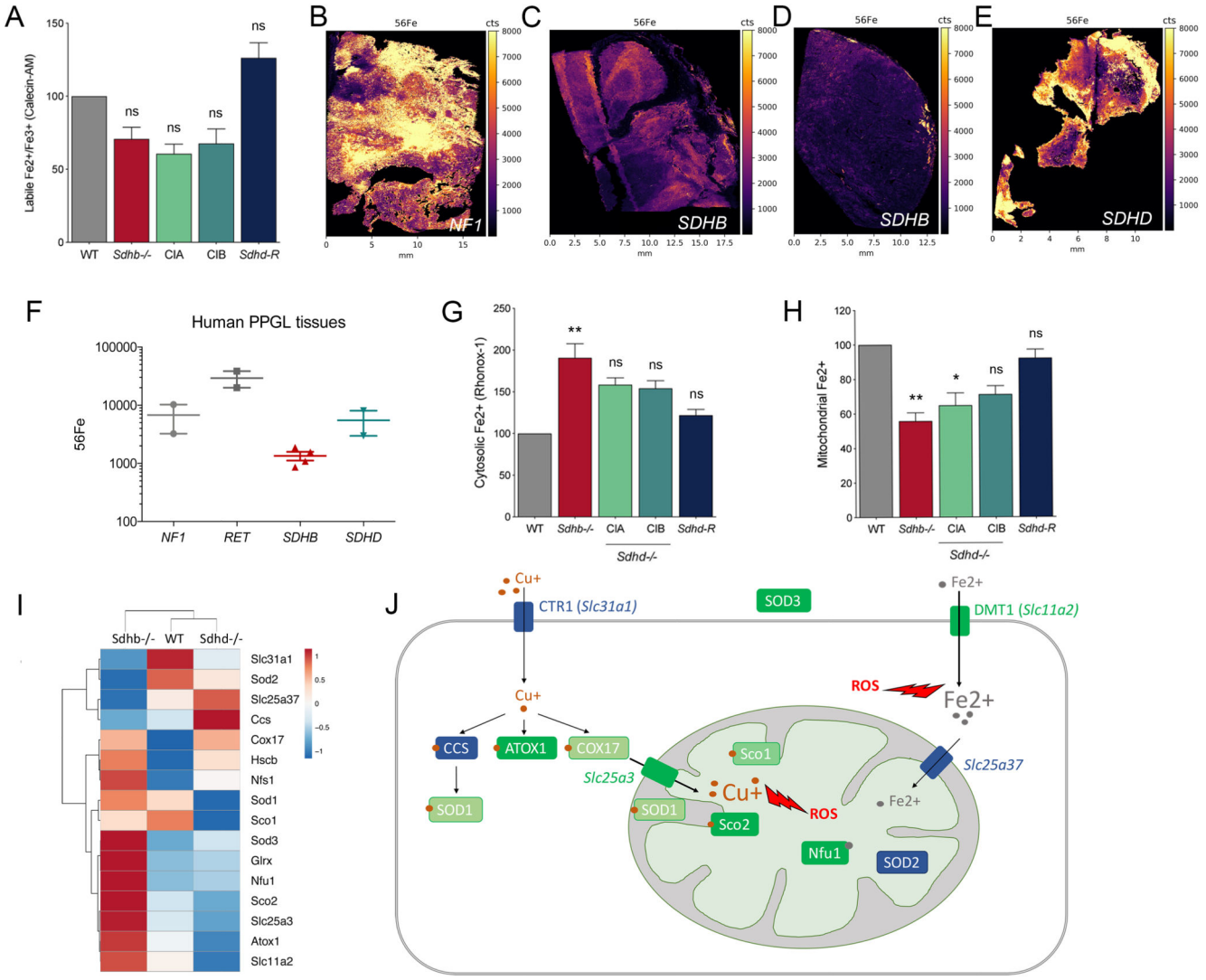

Figure 4. SDH-deficient cells exhibit significant alterations in iron homeostasis, notably marked in *Sdhb* KO cells.

A, Flow cytometry analysis of labile overall iron content in each cell line. **B,** Representative ^{56}Fe images generated by LA-ICP-MS in one *NF1*-mutated human pheochromocytoma **C,** one *SDHB*-mutated pheochromocytoma **D,** one *SDHB*-mutated paraganglioma and **E**, one *SDHD*-mutated paraganglioma. Images are displayed using the same threshold to enable a direct visual comparison between tumor sections. Average ^{56}Fe counts in 2 NF1, 2 RET, 4 SDHB and 2 SDHD tumors are shown in **F. G,** Cytosolic Iron(II) content, **H,** mitochondrial Iron(II) content. **I,** Heatmap representation of the expression profiles of several critical actors of iron/copper homeostasis in *Sdhb-/-*, WT and *Sdhd-/-* cells, using mean level values to perform unsupervised classification. **J,** Diagram highlighting the role played by some iron and copper transporters (DMT1, Slc25a37, CTR1 and Slc25a3) explaining the major alterations induced by *Sdhb* KO in their iron and copper cellular homeostasis. Data shown in **A, G** and **H** are from three independent experiments, presented as mean ± SEM. Non-

parametric one-way ANOVA was used to assess statistical significance; ns, not significant, *P≤0.05, **P≤0.01, ***P≤0.001.

Europe PMC Funders Author Manuscripts

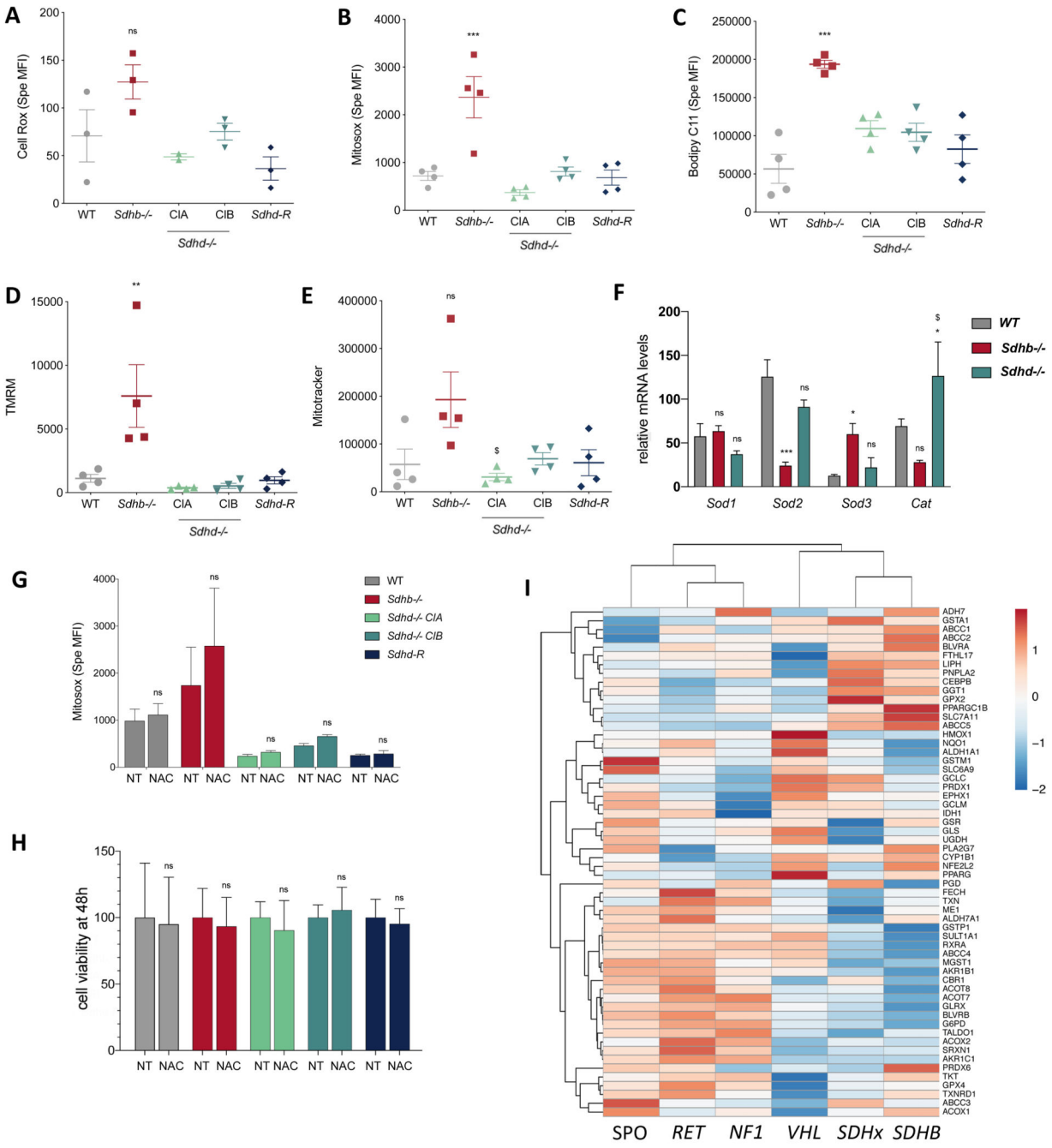

Figure 5. SDHB-deficient cells display increased ROS levels without activation of the NRF2 pathway.

A, Specific MFI using CellROX probe in all imCC cell types. Similar assays were carried out using **B**, Mitosox **C**, Bodipy C11 probe **D**, TMRM and **E**, Mitotracker probes. **F,** RNA-seq analysis showing the mRNA levels of the different forms of superoxide dismutase (cytoplasmic SOD1, mitochondrial and extracellular SOD3) and catalase. **G,** Specific MFI of MitoSOX probe in all imCC models following N-acetyl-cysteine (NAC) treatment (3 mM) for 48h. **H,** Cell survival percentage of indicated cell lines after treatment with 3 mM

Europe PMC Funders Author Manuscripts

of NAC in comparison to vehicle-treated controls for 48h. **I,** Heatmap representation of the expression of 58 NRF2-target genes through the transcriptome data of the COMETE collection of human PPGL. Mean values of NRF2 targets levels in the groups of sporadic non-mutated tumors (n=49), *RET*- (n=19), *NF1*- (n=37), *VHL*- (n=40), *SDHA*, *C*, *D*- (n=6) and *SDHB*-mutated tumors (n=17) were used to perform unsupervised classification. Data shown in **A, B, C, D** and **E** each dot is representative of an independent experiment (n=4), bar plots show means ± SEM. One-way ANOVA was used to assess statistical significance; ns, not significant, *P≤0.05, **P≤0.01, ***P≤0.001 relative to WT and $P≤0.05 relative to *Sdhb-/-* imCC. In **G** and **H** results shown are from at least three independent experiments and presented as means ± SEM. To assess statistical significance in **F, G** and **H**, Two-way ANOVA was used; ns, not significant, *P≤0.05, ***P≤0.001.

Europe PMC Funders Author Manuscripts

Europe PMC Funders Author Manuscripts

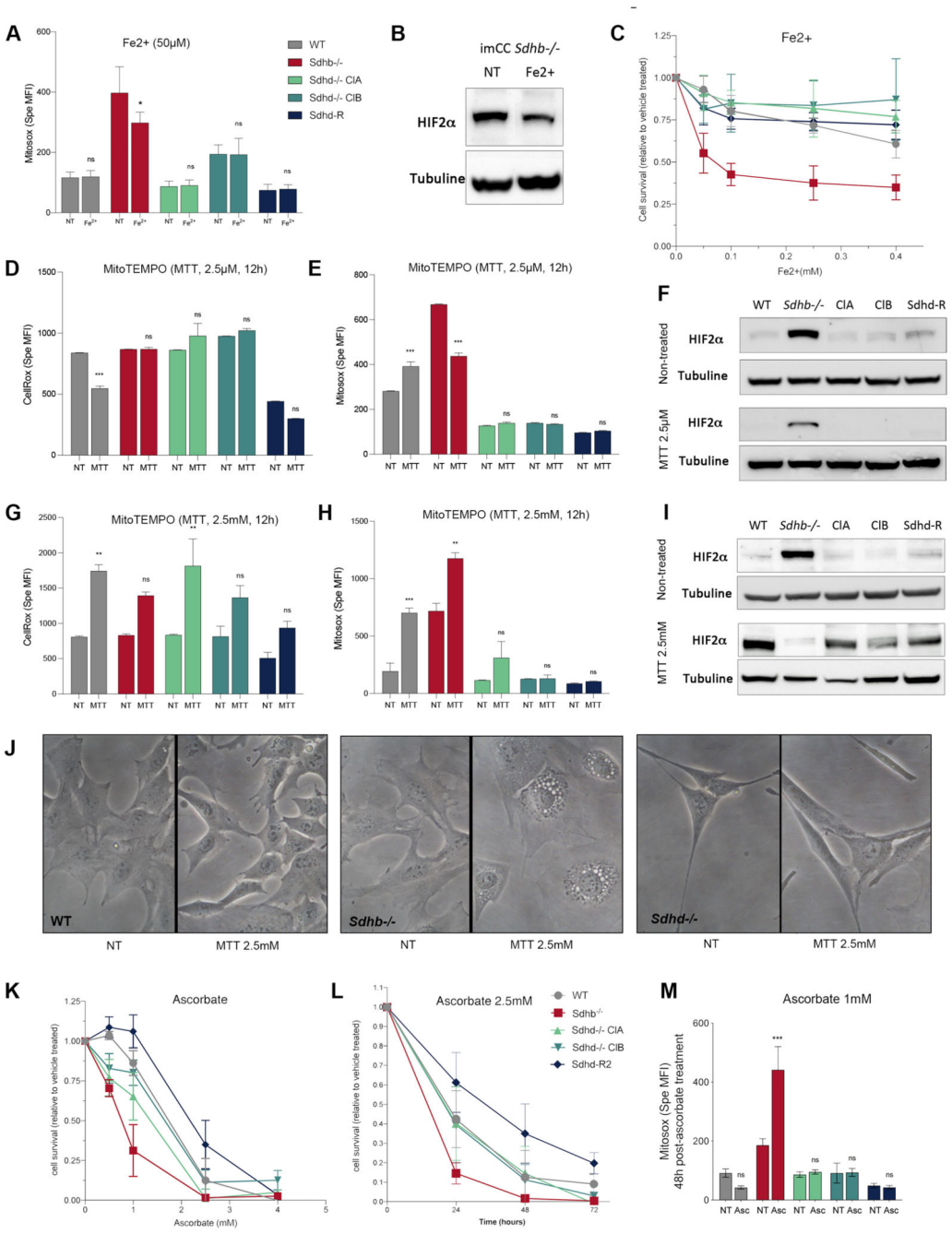

Figure 6. Modulation of Iron(II) and ROS levels affects HIF2α stabilization and survival in Sdhb-deficient cells.

A, Specific MFI of MitoSOX probe in all imCC models following treatment for 48h with either Iron(II) 50μM or vehicle. **B,** Western blot of HIF2α in total cellular extracts of *Sdhb-/-* imCCs not-treated (NT) or treated for 48h with Iron(II) (Fe^{2+}). **C,** Dose-response curves showing cell survival of all cell types following 48h of treatment with Iron(II). **D,** Specific MFI of CellROX probe in all imCC models following treatment for 12 hours with MitoTEMPO (MTT) 2.5 μM in comparison to NT cells. **E,** Same as **D,** using MitoSOX

probe. **F,** Western blot of HIF2α in total cellular extracts NT or treated for 12h with 2.5 μM MTT. **G,** Same as **D,** after treatment with MTT 2.5 mM. **H,** Same as **G,** using MitoSOX probe. **I,** Same as **F,** after treatment for 12h with 2.5 mM MTT. **J,** Cell morphology following treatment for 12h with MTT 2.5 mM. **K,** Same as **C** following Ascorbate treatment. **L,** Time-response curves showing cell survival of all imCC models after treatment with 2.5 mM ascorbate. **M,** Specific MFI of MitoSOX probe in all imCC models following treatment for 48h with either ascorbate 1mM or vehicle. Data for **C, K,** and **L** are all relative to vehicle-treated controls and presented as means ± SEM (n = 3 independent experiments, with 3 technical replicates/experiment). Data from **A,** and **M** are mean of at least three independent experiments and data from **D, E, G,** and **H** are mean of at least two independent experiments. Data are presented as mean ± SEM and two-way ANOVA was performed; ns, not significant, *P≤0.05, ***P≤0.001.